7-2015

Synthesis of Palladium and Palladium-Copper Nanostructures as Electrocatalysts

Haibin Wu
University of Arkansas, Fayetteville

Synthesis of Palladium and Palladium-Copper Nanostructures as Electrocatalysts

A thesis submitted in partial fulfillment
of the requirements for the degree of
Master of Science in Chemistry

By

Haibin Wu
Lanzhou University
Bachelor of Science in Chemistry, 2010

July 2015
University of Arkansas

This thesis is approved for recommendation to the Graduate Council.

_____

Dr. Jingyi Chen
Committee Chairperson

_____

Dr. Ingrid Fritsch
Committee Member

_____

Dr. Feng Wang
Committee Member

ABSTRACT

Pd and its alloys are alternatives of Pt as promising catalysts and electrocatalysts for many reactions. Size controlled synthesis of nanoparticles remains a major research subject, since smaller size particles show better catalytic performance. In this work, we developed a modified chemical wet method to prepare Pd and Pd-Cu nanostructures with uniform small size. Different sizes and shapes of Pd nanostructures were successfully synthesized by using the two reducing agents (i.e., L-ascorbyl-6-palmitate or phenylphosphinic acid). The reducing agents play a role to control the final morphologies and sizes of particles. The use of L-ascorbyl-6-palmitate favors to form irregular branch shapes or rods; in contrast, the use of phenylphosphinic acid tends to form spherical nanoparticles. Furthermore, phenylphosphinic acid can assist with size control of Pd particles. Co-reducing Pd and Cu precursors can obtain Pd-Cu nanostructures with different sizes and shapes. The growth mechanism is followed the deposition of Cu on Pd seeds which are reduced prior to Cu. Similar to pure Pd synthesis, phenylphosphinic acid reduced the precursors to form small uniform spherical particles compared to L-ascorbyl-6-palmitate. It was also found that the composition could also be tuned by using different reducing agents. The catalytic activity of Pd and Pd-Cu nanostructures for ethanol oxidation reaction (EOR) has been tested in basic solution for alkaline fuel cell applications. The specific areas of these Pd and Pd-Cu are much higher than those reported previously. It was found that both Pd and Pd-Cu nanostructures exhibited enhanced catalytic activities and to some extent resisted CO-like intermediates poisoning. Most catalysts had enhanced current densities after 500 cycle scan, indicating enhanced stability of those catalysts.

ACKNOWLEDGEMENTS

Firstly I would like to thank my mother for all her support and encouragement. Every important decision I made in my life is totally supported by my mother, even though some of them sounded ridicules.

I would like to express my deep appreciation to my advisor Dr. Jingyi Chen for her continuous support of my study and research, for her patience and immense knowledge. In the past three years, I got learned a lot from her, like attitude to work and study skills. During thesis preparation, I got a lot of help and useful suggestions from her.

Also, I would like to thank my committee members. Dr. Ingrid Fritsch, your class was the first class I took at University of Arkansas. It helped me to open my eyes to research about energy in which I have so much interest. Dr. Feng Wang, thank you for your patience and insightful comments for my research.

Next, I appreciate all help from all Chen group members, Samir Jenkins, Leanne Murthrin, and Cameron Crane in research and English. I really enjoyed working with you all in these years. You guys spent your precious time with me on practicing my speaking. The discussion among us helped me find new ways to solve problems I met in class and research.

Last but not the least, I would like to say thank you to my friends here for your encouragement, help, and support. You guys give me three years delight time to live in Fayetteville. Special thanks to Dr. Shutang Chen, you are a great friend and colleague. I enjoyed being friends with you and your family. I was impressed with your selflessness to your friends. Also, I want to say thank you to my friend Jiang Wang for his help and support from college to now.

TABLE OF CONTENTS

LIST OF ABBREVIATIONS

$Pd(acac)_2$	Palladium(II) Acetylacetonate
$Cu(acac)_2$	Copper(II) Acetylacetonate
$CuCl_2$	Copper Chloride
HAc	Acetic Acid
PVP	Poly(vinylpyrrolidone)
Ag/AgCl	Silver / Silver Chloride
EtOH	Ethanol
MeOH	Methanol
MOR	Methanol Oxidation Reaction
EOR	Ethanol Oxidation Reaction
ORR	Oxygen Reduction Reaction
TEM	Transmission Electron Microscopy
PXRD	Powder X-ray Diffraction
UV-vis	Ultra Violate-visible
CV	Cyclic Voltammetry
CA	Chronoamperometry
ECSA	Electrochemical Surface Area
ESA	Specific Surface Area
PEMFC	Proton Exchange Membrane Fuel Cell
ICP-MS	Inductively Coupled Plasma Mass Spectrometry
Pd-Cu	Palladium-Copper Nanostructures
Pd/C	Carbon supported palladium nanoparticles

1. Introduction

1.1 Noble Metal Nanostructures

1.1.1 Pure Noble Metal Nanostructure Catalysts

Owing to their unique and excellent properties, noble metals nanostructures are widely applied in energy conversion and storage,[1-5] catalysis,[9] and gas detection.[10,11] Particularly, noble metals like Pt and Pd and their alloys exhibit high performance and promising applications in catalysis and electrocatalysis. For example, Nørskov *et al*. first developed a method by using density functional theory to study free-energy landscape of oxygen reduction on Pt (111).[13] They also calculated bond energies of oxygen and hydroxyl group on other metals, and by combining these results they constructed a volcano curve, indicating that Pt is the best catalyst for oxygen reduction reaction compared to palladium,[14] iridium,[15] ruthenium,[16] and silver[17]. In addition, these metals have also been used for anodic reactions in fuel cells such as alcohol oxidation.[18-20] On the other hand, metal nanoparticles can also be catalysts for organic reactions such as hydrosilylation reactions, oxidation, C-C coupling reaction, and hydrogenation.[21] For example, Ag nanoparticles catalyzed coupling of alcohols was reported by Shimizu and his co-workers.[22] On the other hand, among these noble metals, Pd is well known as a good type of material to store hydrogen. Campesi *et al*. successfully improved hydrogen adsorption through nanosize palladium structure on porous carbon.[23] Because of various applications and prominent performance as catalysts, metal nanostructures, especially noble metals, have been intensively studied in the past decades.

1.1.2 Bimetallic Nanoparticles

Even though pure noble metals display excellent performances on catalysis, the limited abundance and high cost of these metals motivate scientists to search for new catalysts or seek for new ways to reduce the cost. Applying bimetallic nanoalloys as substitutes for pure noble metals is a practical strategy to reduce use of noble metals while maintaining performance. Bimetallic nanoalloys are the metals consisting of two metal elements at nanoscale. The structures of bimetallic nanoalloys are divided into four main types: core-shell segregated nanoalloys, subcluster segregated nanoalloys, mixed A-B nanoalloys, and multishell nanoalloys, the structures of which are shown in Figure 1-1. These mixing patterns, to some degree, determine morphologies of nanoalloys. Furthermore, Ferrando *et al*. pointed out the factors influencing mixing patterns in nanoalloys,[6] including relative bond strength between the two metal elements, surface energies of the bulk metals, relative atomic sizes, charge transfer, bonds strength between surfactant and surface atoms, and other specific electronic/magnetic effects.

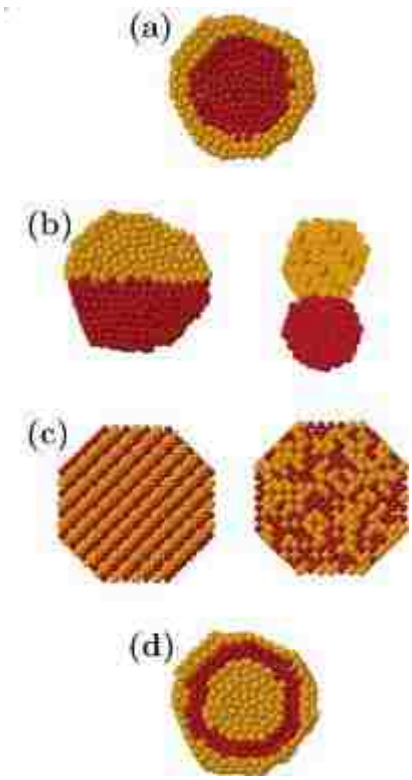

1.1.3 Synthesis of Metal Nanostructures

1.1.3.1 Synthetic Strategies

Since the first study about metal particles was reported by Michael Faraday in 1857,[24] researchers have applied many synthetic methods to obtain metal particles. The typical synthetic strategies for bottom-up solution synthesis are mainly the following four methods: *a)* chemical reduction, *b)* thermal decomposition of some metal precursors, *c)* electrochemical synthesis, and *d)* sonochemical synthesis.[25] For bimetallic nanoalloys, chemical reduction is furthermore classified into these three approaches: *(i)* co-reduction, *(ii)* reduction of bimetallic complex, and *(iii)* successive reduction including template/seed synthesis, which is to form second metal on the pre-formed nanostructures.[25]

(a) Chemical reduction: For examples, strong aqueous reducing agents, such as $NaBH_4$, were applied to form metal nanostructures in the presence of surfactants acting to protecting ligands to stabilize nanostructures. Monodesperse nanostructures of these noble metals (*eg.* Au, Ag, Pt ,and Pd) have been well studied.[12] Due to well-known stability and biocompatibility of Au, the synthetic methods of its nanostructures have been well studied. For instance, Li *et al*. modified polyol process to develop high-yield synthesis of single-crystalline gold octahedral.[26] In the synthetic process, the reducing agent $NaBH_4$, was mixed in the solution of polyethylene glycol (M.W.=600) containing polyvinylpyrrolidone (PVP), and then the aqueous $AuCl_3$ solution was added in the mixture and was maintained for 24 h for crystallization. Han *et al*. prepared controlled size and morphology Au particles with a reactive templated method.[27] In the process of chemical reduction, the effect of trace amount of some inorganic salt on morphology has been noticed.[28] Xiong *et al*. also studied the function of PVP in the chemical reduction process to form the morphologies of noble metal particles (Ag, Au, Pt, and Pd).[29] They believed that hydroxyl

group of PVP could reduce the metal salts slowly enough, resulting in kinetically controlled growth.

Noble metal particles can be also prepared in organic solvents such as dimethylformamide (DMF). Those solvents have a multifunctional role in the process of formation of metal nanoparticles. Those molecules are weak reducing agents which donate electrons to metal precursors. Except such small molecules as DMF, other long-chain primary alkyl amines, such as oleylamine, octadecylamine or hexadecylamine are frequent to apply in nanoparticle synthesis. Those long-chain amines not only serve as solvents but can also adsorb on the surfaces of nanostructures to passivate the particles as stabilized ligands. For instance, Lacroix *et al*. used H_2PtCl_4 as a precursor to yield unprecedented shapes of Pt nanoparticles in oleylamine.[30] Pazos-Pe´rez *et al*. reported a simplified procedure to generate ultrathin gold single crystal nanowires, in the process of formation of nanowires oleylamine plays a role of shape-directing agent.[31]

Bimetallic nanoalloys can be synthesized by co-reduction. In co-reduction process, the precursors of different metals are reduced by reducing agents, but due to different activity of metals, the one that has higher redox potential forms a core for the other one to deposit.[6] Reduction of bimetallic complex is a sub-category of chemical reduction. Such reduction is similar to co-reduction process, but the precursors in this one are complexes containing two metal species. For example, silver (I) bis (oxalato) palladate (II) was used as a precursor to form Ag-Pd colloid by photoreduction.[32] On the other hand, successive reduction is useful for some specific morphologies such as core-shell structures. The three-layers Au-Pd nanoparticles were produced through successive reduction of the monometallic elements.[33] Rodr´ıguez-Gonza´lez *et*

al. in their report, synthesized multishell bimetallic AuAg nanoparticles by successive reduction of $AgNO_3$ and $HAuCl_4$ in the presence of ligands.[34]

(b) Thermal decomposition of metal precursors: Thermal decomposition of appropriate precursors is a common way to obtain some metal particles, especially in organic synthetic phases, in which synthetic temperature can even reach above 300 ℃ depending on choice of organic solvents. For example, thermal decomposition of Pd-TOP (trioctaphosphine) can be used to obtain Pd particles with uniform sizes from 3.5-7 nm at 300 ℃.[35] At such high temperature, some active metals particles can be also synthesized. Kim *et al.* decomposed Fe- (II)-stearate complex in oleic acid at 380 ℃ to form hollow nanoframes of uniform 21 nm.[36] This method, however, has an disadvantage: at relatively low temperature the precursors could not decompose, but at high temperature such as 400 ℃ the organic ligands, such as oleic acid, would completely decompose resulting in aggregation of particles. For those metals which are not strong oxidizers as Au, Pt or Pd, another commonly-

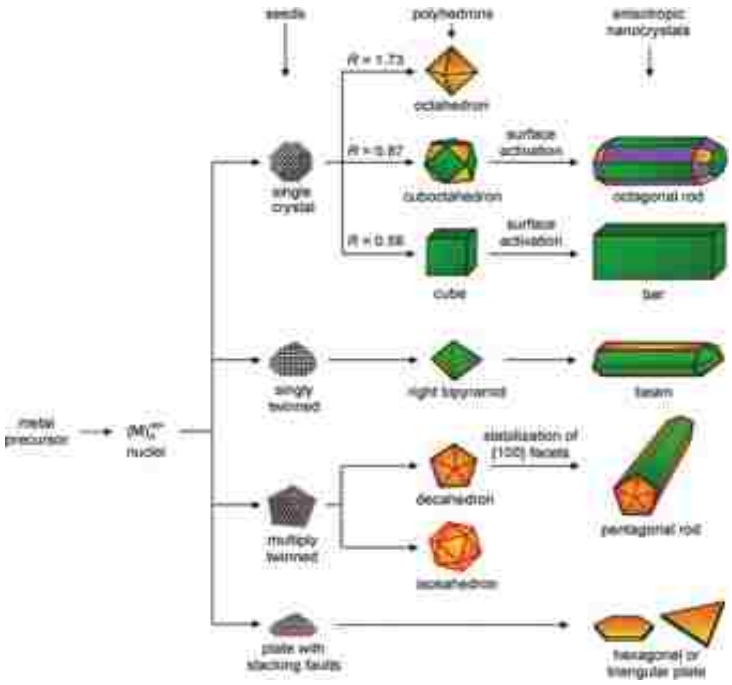

used method to prepare those metal particles is to thermolysis of zero-valence metal complex, such as metal carbonyl. The usage of $Fe(CO)_5$ could lower the synthetic temperature below 300 ℃.[37] Gao *et al*. prepared Co nanoparticles by thermal decomposition of $Co_2(CO)_8$ passivated by triphenylphosphine and oleic acid.[38] The nuclei of Co particles formed at 220 ℃ very rapidly with releasing CO gas, and then the reaction was kept at 185 ℃ for 20 min to crystallize. Such method is also used to prepare bimetallic nanoalloys. Su *et al*. successfully thermally-decomposed $Fe(CO)_5$ and $Pt(acac)_2$ to synthesize FePt nanoalloys.[39]

(c) Electrochemical synthesis: electrochemical synthesis is the synthesis using an electrochemical cell, in which chemical reactions are induced by the added voltages. In comparison with chemical wet methods, electrochemical synthesis to some degree may generate "surface clean" structures. Guo *et al*. developed low cost electrochemical route to produce diameter-controlled hierarchical flowerlike gold microstructures without surfatants.[40] Apart from this advantage, electrochemical synthesis can generate high-index faceted nanostructures, which are thought to have high catalytic activity. A square-wave potential method was applied to obtain high-index faceted Pt nanocrystals.[41] Periodic oxygen adsorption and desorption is critical to shape Pt nanocrysal surfaces.

(d) Sonochemical synthesis: sonochemical synthesis is a way to utilize high power ultrasound to induce chemical reactions.[25] With the assistance of ultrasound, some reactions can occur easily at low temperature. Iron nanoparticles were produced by sonochemical synthesis.[42] Compared to chemical reduction,[37] high power ultrasound could decompose $Fe(CO)_5$ at surprisingly low at 20 ℃. In addition, the mixture of $NaAuCl_4 \bullet 2H_2O$, $PdCl_2 \bullet 2NaCl \bullet 3H_2O$, and sodium dodecyl sulfate was sonicated for Au-Pd bimetallic nanoparticles.[43]

1.1.3.2 Shape Control of Metal Particles

Morphology is a key factor influencing the properties of nanostructures. Xia and his co-worker wrote a comprehensive review paper to summarize the shape-controlled synthesis of metal nanocrystals.[12] Metal nanostructures have been synthesized in various shapes including sphere, cube, cuboctahedron, octahedron, tetrahedron, icosahedron, rod or wire etc. The nucleation is the very beginning stage of crystal growth for the formation of either bulk or nanomaterials. At this stage, metal precursor compounds are decomposed or reduced to zero valence atoms, and these atoms assemble together to form the initial nuclei. As a nucleus grows past the critical size, the cluster will form a well-defined structure as a seed. The further evolution from seeds forms the final shapes of nanostructures. The reaction pathways leading to different shapes of face-centered cubic metals are shown in Figure 1-2.[12]

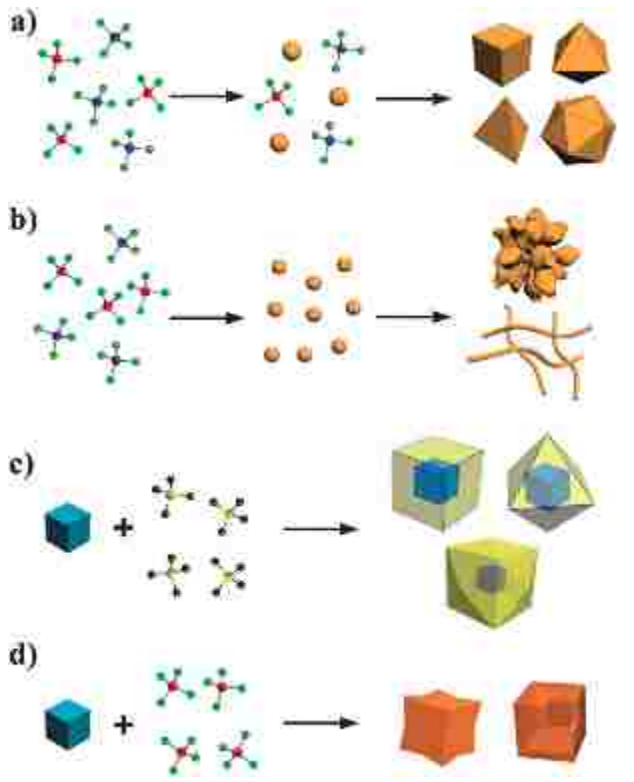

1.1.3.2 Routes to Shape Controlled Bimetallic Nanostructures

The formation of shaped controlled nanostructures involves nucleation and crystal growth. Gu et al. in their review paper summarized four routes to obtain shape controlled bimetallic

nanocatalysts.[8] Figure 1-3 shows the four routes towards shape-controlled bimetallic nanocrystals. The first two routes proceed in one-pot method, in which two different metal precursors mix together at the beginning of the synthesis. In both of these two routes, the small bimetallic nuclei or seeds form first in the reaction. In the first route, metal precursors, however, are continuously reduced and added to the nuclei, and the nuclei grow bigger and form uniform shapes, in Figure 1-3a. The second route displays a different behavior, in which the nuclei directly aggregate together and regrow to one-dimensional or dendritic structures. In the latter two routes, before reduction of second metal precursors, the primary metal seeds already exit in the reactive system which is known as seeded growth. The seeded growth route shown in Figure 1-3c, the second metal precursor is reduced by solvents or added reducing agents. The reduced metal deposits on the seed, resulting in a core-shell structure. In some cases, due to diffusion of atoms, this route may lead to mixed bimetallic nanocrystals.[9] In a galvanic replacement process shown in Figure 1-3d, the second metal will partially take place of the atoms in the seeds, which means that dissolution of seed atoms and deposition of second metal atoms occur simultaneously. In this route, it is easy to obtain concave or hollow structures. Based on the features of these four routes, the first two routes are known as co-reduction strategies; the latter two are considered as successive reductions.

1.2 Catalytic Applications

1.2.1 Background of Fuel Cells

Generally speaking, fuel cells are the device to convert chemical energy to electric work with less pollution and high energy conversion efficiency. Fuel cells are known for at least 150 years, and they have already been applied in many fields. For example, in 1960's fuel cells were used in NASA's space missions, such as the Apollo Program. There are various types of fuel

cells; however, the basic structure of fuel cells comprises anode electrodes where fuels are oxidized, cathode electrodes where pure oxygen or oxygen in air is reduced to form water, and electrolytes which allow charges to move from one electrode to the other one. Fuel cells can be classified in term of electrodes, types of fuels, operating temperatures, membranes etc., such as alkaline fuel cell (AFC), proton exchange membrane fuel cell (PEMFC), direct methanol fuel cell (DMFC), phosphoric acid fuel cell (PAFC), molten carbonate fuel cell (MCFC), and solid oxide fuel cell (SOFC) shown in Figure 1-4.[7] Even though hydrogen has a very high specific energy density ~ 142 MJ/kg, the storage of and generation of hydrogen in a large scale is a challenge. In comparison to hydrongen, common organic fuels are good options. Following hydrogen, methanol is another promising candidate fuel in fuel cells. The fuel cell with direct use of methanol is called direct methanol fuel cell (DMFC). Typical environment where DMFC is acidic, although in alkaline environments kinetics can be faster, carbonate will form in basic solution.[7] The widely-used catalysts for DMFC are noble metals, namely Pt or Pt based catalysts. The process of methanol oxidation on the surface of Pt contains adsorption of methanol on the surface, insertion oxygen in the molecule to form intermediates, such as CO, then further

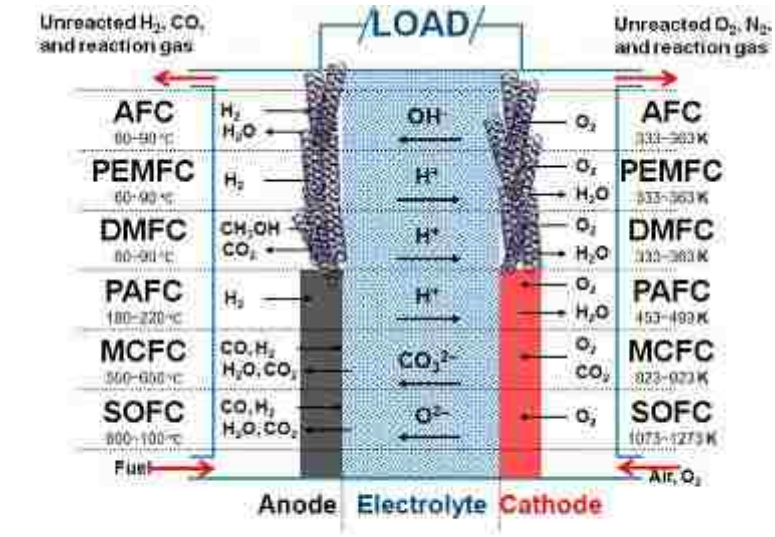

oxidization of the intermediates to generate final product CO_2, and then desorption of CO_2. As is well known, CO can tightly bond to Pt atoms so that it can occupy the active sites of catalysts. This consequently leads to the loss of activity of catalyst, which is called catalyst poisoning. Compared to methanol, ethanol can cause less catalysts poisoning, and have higher specific energy density. The summary of the global oxidation mechanism of ethanol in an acidic environment can be described as follow:[44]

$$CH_3CH_2OH \rightarrow [CH_3CH_2OH]_{ad} \rightarrow C1_{ad}, C2_{ad} \rightarrow CO_2 \text{ (total oxidation)} \quad (1)$$

$$CH_3CH_2OH \rightarrow [CH_3CH_2OH]_{ad} \rightarrow CH_3CHO \rightarrow CH_3COOH \text{ (partial oxidation)} \quad (2)$$

$C1_{ad}$ and $C2_{ad}$ represent two distinct oxidation pathways where the adsorbed intermediates are one or two carbons molecules, respectively. In addition, the investigation from Wang *et al*. tested a few alcohols for fuel cells, and they commented that ethanol was promising alternative of methanol as fuel.[45] They analyzed the electrooxidation products on mass spectrum and pointed that the increasing water/ethanol ratio could contribute to formation of CO_2.

One of the key parts of fuel cells is the material of electrodes. Pt and Pt based catalysts are still extensively used in acidic solution as anodic catalysts for ethanol oxidation;[46-48] however, due to easily poisoned by CO-like intermediates, Pt species catalysts have relatively low performance. The application of Pd and Pd-based catalysts can to some degree avoid the disadvantages of Pt-based catalysts, especially in alkaline solution.[49] Recently, Pd and Pd-based nanostructures have been widely studied for EOR as anodic catalysts. Wang *et al.* reported Pd supported by multiwall carbon nanotubes displayed high efficiency on EOR with the highest

peak current density of 1.23 A/mg $_{Pd}$.[50] Compared to pure Pd catalysts, Pd-based bimetallic catalysts have better catalytic activity, like PdAu,[51] PdAg,[52] Pd-Cu[53,54] etc. Among those bimetallic catalysts, Pd-Cu seems a potential alternative for pure noble metal catalysts, due to its relatively low cost. Mukherjee *et al*. found that after alloying Cu, Pd-Cu showed higher current density and better resistance against CO-like intermediate poisoning as EOR catalysts.[53]

1.2.2 CO_2 Electrochemical Reduction

Due to burning fossil fuels, more and more greenhouse gases are released into atmosphere, which results in serious climate change. Among those greenhouse gases, CO_2 makes big contribution to global warming. Therefore, based the goal to keep the balance of CO_2 in air and relief the human's high demand of energy, converting CO_2 to some fuel molecules is practical and critical. Currently, conversion of CO_2 can be achieved through chemical, electrocatalytic, and photocatalytic methods. Owing to its advantages such as controllable process by temperature and electrode potential, electrochemical reduction of CO_2 to low carbon fuel molecules attracts much research attention.[55] The different pathways of electrochemical reduction of CO_2 can result in different products. The major products are CO, methane, methanol, ethanol, formic acid, oxalic acid etc. The mechanism and kinetics study reveals that oxalate formation via the self-coupling of carbon dioxide radicals (CO_2^{-*}), formate formation via protonation of CO_2^{-*} and CO formation via oxygen-carbon coupling of CO_2^{-*}; therefore, the key step of reduction CO_2 is to form CO_2^{-*}.[56] However, as a result of the very negative redox potential of formation of CO_2^{-*}~ -1.9 V, CO_2 reduction has high barrier requiring more negative potential to generate final products. Some transition metals oxides have been applied for CO_2 reduction as electrodes. Brandi *et al*. used mixed metallic oxides including RuO_2, TiO_2, MoO_2, Co_3O_4, and Rh_2O_3 to achieve low overpotentials of reduction of CO_2.[57] In addition, metal

complexes are also widely applied for CO_2 reduction, Cr(III)–TPPCl,[58] fac-(5,50-bisphenylethynyl-2,20-bipyridyl)$Re(CO)_3Cl$,[59] CoIITPP or CoTPP-py-NHCO[58] *etc*. Another type of material for CO_2 reduction is a pure metal, such as Cu and Pd. The exploration of CO_2 reduction on Cu electrodes was reported in 1985-1986.[60] A current efficiency for methane was reported as high as 65% on Cu electrodes even at 0 ℃.[61] Cu and its oxide Cu_2O showed excellent performance on CO_2 reduction. Recently, Li *et al.* found that Cu particles synthesized by reducing Cu_2O could reduce CO_2 at exceptionally low overpotentials.[62] Ohkawa *et al*. carried out CO_2 reduction exploration on Pd electrodes.[63-65] In their work, the current efficiency was increased by adding Cu to Pd electrodes. The enhancement of catalytic performance was thought the participation of adsorbed hydrogen. In Kolbe and its co-workers work, they pointed that conversion of CO_2 to CO occurred -1 V vs SHE (standard hydrogen electrode).[66] Hoshi *et al*. demonstrated that Pd (111) surface showed the higher activity than Pd (100) surface, which was in contrast to other Pt group metals, like Pt, Ir.[67] However, the main challenges of CO_2 reduction are still high activation energy and large overpotentials, and thus low energy efficiency.

1.3 Objectives

As is discussed, Pt is widely applied as catalyst in many areas, but the low resistance against CO-like intermediate poisoning and high cost motivate scientists to search the alternative of Pt. The activity and oxygen bond energy of Pd is close to Pt, so it is believed that Pd is a promising material to replace the Pt to some degree. Further studies about anodic reactions on metal electrodes revealed that Pd-based catalysts exhibited higher activity than Pt on EOR in alkaline environment. After literature review about CO_2 reduction, we have identified that Pd-Cu might be a good catalyst for CO_2 reduction due to high adsorption of hydrogen on Pd surface.

This work aims to develop synthetic strategy to obtain Pd and Pd-Cu nanostructures. To this end, we employed phenylphosphinic acid and L-ascorbyl-6-palmitate as reducing agents to obtain Pd and Pd-Cu nanostructures. Through combining different Cu precursors ($CuCl_2$ or $Cu(acac)_2$) with reducing agents, the size and morphology of the resulting nanocrystals could be tuned. We further characterized the catalytic activity of these nanostructures for both EOR. For EOR, we found that the catalysts had very large specific active areas, indicating that they may be high efficient catalysts for EOR.

1.4 References

(1) Nie, Y.; Li, L.; Wei, Z. *Chemical Society Reviews* **2015**, *44*, 2168.

(2) Bambagioni, V.; Bianchini, C.; Marchionni, A.; Filippi, J.; Vizza, F.; Teddy, J.; Serp, P.; Zhiani, M. *Journal of Power Sources* **2009**, *190*, 241.

(3) Yajima, T.; Wakabayashi, N.; Uchida, H.; Watanabe, M. *Chemical Communications* **2003**, 828.

(4) Park, K.-W.; Choi, J.-H.; Kwon, B.-K.; Lee, S.-A.; Sung, Y.-E.; Ha, H.-Y.; Hong, S.-A.; Kim, H.; Wieckowski, A. *The Journal of Physical Chemistry B* **2002**, *106*, 1869.

(5) Zhu, W.; Michalsky, R.; Metin, O.; Lv, H.; Guo, S.; Wright, C. J.; Sun, X.; Peterson, A. A.; Sun, S. *Journal of the American Chemical Society* **2013**, *135*, 16833.

(6) Ferrando, R.; Jellinek, J.; Johnston, R. L. *Chemical Reviews* **2008**, *108*, 845.

(7) Kakati, N.; Maiti, J.; Lee, S. H.; Jee, S. H.; Viswanathan, B.; Yoon, Y. S. *Chemical Reviews* **2014**, *114*, 12397.

(8) Gu, J.; Zhang, Y.-W.; Tao, F. *Chemical Society Reviews* **2012**, *41*, 8050.

(9) Chen, S.; Jenkins, S. V.; Tao, J.; Zhu, Y.; Chen, J. *The Journal of Physical Chemistry C* **2013**, *117*, 8924.

(10) Kolmakov, A.; Klenov, D. O.; Lilach, Y.; Stemmer, S.; Moskovits, M. *Nano Letters* **2005**, *5*, 667.

(11) Yang, D.; Carpena-Nunez, J.; Fonseca, L. F.; Biaggi-Labiosa, A.; Hunter, G. W. *Sci. Rep.* **2014**, *4*.

(12) Xia, Y.; Xiong, Y.; Lim, B.; Skrabalak, S. E. *Angewandte Chemie International Edition* **2009**, *48*, 60.

(13) Nørskov, J. K.; Rossmeisl, J.; Logadottir, A.; Lindqvist, L.; Kitchin, J. R.; Bligaard, T.; Jónsson, H. *The Journal of Physical Chemistry B* **2004**, *108*, 17886.

(14) Pires, F. I.; Villullas, H. M. *International Journal of Hydrogen Energy* **2012**, *37*, 17052.

(15) Qiao, J.; Lin, R.; Li, B.; Ma, J.; Liu, J. *Electrochimica Acta* **2010**, *55*, 8490.

(16) Zaikovskii, V. I.; Nagabhushana, K. S.; Kriventsov, V. V.; Loponov, K. N.; Cherepanova, S. V.; Kvon, R. I.; Bönnemann, H.; Kochubey, D. I.; Savinova, E. R. *The Journal of Physical Chemistry B* **2006**, *110*, 6881.

(17) Zhou, R.; Qiao, S. Z. *Chemistry of Materials* **2014**, *26*, 5868.

(18) Bianchini, C.; Shen, P. K. *Chemical Reviews* **2009**, *109*, 4183.

(19) Xu, C.; Tian, Z.; Shen, P.; Jiang, S. P. *Electrochimica Acta* **2008**, *53*, 2610.

(20) Hu, F. P.; Shen, P. K.; Li, Y. L.; Liang, J. Y.; Wu, J.; Bao, Q. L.; Li, C. M.; Wei, Z. D. *Fuel Cells* **2008**, *8*, 429.

(21) Roucoux, A.; Schulz, J.; Patin, H. *Chemical Reviews* **2002**, *102*, 3757.

(22) Shimizu, K.-i.; Sato, R.; Satsuma, A. *Angewandte Chemie International Edition* **2009**, *48*, 3982.

(23) Campesi, R.; Cuevas, F.; Gadiou, R.; Leroy, E.; Hirscher, M.; Vix-Guterl, C.; Latroche, M. *Carbon* **2008**, *46*, 206.

(24) Faraday, M. *Philosophical Transactions of the Royal Society of London* **1857**, *147*, 145.

(25) Sankar, M.; Dimitratos, N.; Miedziak, P. J.; Wells, P. P.; Kiely, C. J.; Hutchings, G. J. *Chemical Society Reviews* **2012**, *41*, 8099.

(26) Li, C.; Shuford, K. L.; Park, Q. H.; Cai, W.; Li, Y.; Lee, E. J.; Cho, S. O. *Angewandte Chemie* **2007**, *119*, 3328.

(27) Han, J.; Liu, Y.; Guo, R. *Advanced Functional Materials* **2009**, *19*, 1112.

(28) Wiley, B.; Herricks, T.; Sun, Y.; Xia, Y. *Nano Letters* **2004**, *4*, 1733.

(29) Xiong, Y.; Washio, I.; Chen, J.; Cai, H.; Li, Z.-Y.; Xia, Y. *Langmuir* **2006**, *22*, 8563.

(30) Lacroix, L.-M.; Gatel, C.; Arenal, R.; Garcia, C.; Lachaize, S.; Blon, T.; Warot-Fonrose, B.; Snoeck, E.; Chaudret, B.; Viau, G. *Angewandte Chemie International Edition* **2012**, *51*, 4690.

(31) Pazos-Pérez, N.; Baranov, D.; Irsen, S.; Hilgendorff, M.; Liz-Marzán, L. M.; Giersig, M. *Langmuir* **2008**, *24*, 9855.

(32) Torigoe, K.; Esumi, K. *Langmuir* **1993**, *9*, 1664.

(33) Ferrer, D.; Torres-Castro, A.; Gao, X.; Sepúlveda-Guzmán, S.; Ortiz-Méndez, U.; José-Yacamán, M. *Nano Letters* **2007**, *7*, 1701.

(34) Rodriguez-Gonzalez, B.; Burrows, A.; Watanabe, M.; Kiely, C. J.; Liz Marzan, L. M. *Journal of Materials Chemistry* **2005**, *15*, 1755.

(35) Kim, S.-W.; Park, J.; Jang, Y.; Chung, Y.; Hwang, S.; Hyeon, T.; Kim, Y. W. *Nano Letters* **2003**, *3*, 1289.

(36) Kim, D.; Park, J.; An, K.; Yang, N.-K.; Park, J.-G.; Hyeon, T. *Journal of the American Chemical Society* **2007**, *129*, 5812.

(37) Farrell, D.; Majetich, S. A.; Wilcoxon, J. P. *The Journal of Physical Chemistry B* **2003**, *107*, 11022.

(38) Yang, H. T.; Shen, C. M.; Wang, Y. G.; Su, Y. K.; Yang, T. Z.; Gao, H. J. *Nanotechnology* **2004**, *15*, 70.

(39) Sun, S.; Murray, C. B.; Weller, D.; Folks, L.; Moser, A. *Science* **2000**, *287*, 1989.

(40) Guo, S.; Wang, L.; Wang, E. *Chemical Communications* **2007**, 3163.

(41) Zhou, Z.-Y.; Huang, Z.-Z.; Chen, D.-J.; Wang, Q.; Tian, N.; Sun, S.-G. *Angewandte Chemie International Edition* **2010**, *49*, 411.

(42) Suslick, K. S.; Fang, M.; Hyeon, T. *Journal of the American Chemical Society* **1996**, *118*, 11960.

(43) Mizukoshi, Y.; Okitsu, K.; Maeda, Y.; Yamamoto, T. A.; Oshima, R.; Nagata, Y. *The Journal of Physical Chemistry B* **1997**, *101*, 7033.

(44) Antolini, E. *Journal of Power Sources* **2007**, *170*, 1.

(45) Wang, J.; Wasmus, S.; Savinell, R. F. *Journal of The Electrochemical Society* **1995**, *142*, 4218.

(46) Ribadeneira, E.; Hoyos, B. A. *Journal of Power Sources* **2008**, *180*, 238.

(47) Prabhuram, J.; Zhao, T. S.; Tang, Z. K.; Chen, R.; Liang, Z. X. *The Journal of Physical Chemistry B* **2006**, *110*, 5245.

(48) Zhang, X.; Zhu, H.; Guo, Z.; Wei, Y.; Wang, F. *Journal of Power Sources* **2011**, *196*, 3048.

(49) Kamarudin, M. Z. F.; Kamarudin, S. K.; Masdar, M. S.; Daud, W. R. W. *International Journal of Hydrogen Energy* **2013**, *38*, 9438.

(50) Wang, Y.; He, Q.; Ding, K.; Wei, H.; Guo, J.; Wang, Q.; O'Connor, R.; Huang, X.; Luo, Z.; Shen, T. D.; Wei, S.; Guo, Z. *Journal of The Electrochemical Society* **2015**, *162*, F755.

(51) Qiu, X.; Dai, Y.; Tang, Y.; Lu, T.; Wei, S.; Chen, Y. *Journal of Power Sources* **2015**, *278*, 430.

(52) Kakaei, K.; Dorraji, M. *Electrochimica Acta* **2014**, *143*, 207.

(53) Mukherjee, P.; Roy, P. S.; Mandal, K.; Bhattacharjee, D.; Dasgupta, S.; Bhattacharya, S. K. *Electrochimica Acta* **2015**, *154*, 447.

(54) Noborikawa, J.; Lau, J.; Ta, J.; Hu, S.; Scudiero, L.; Derakhshan, S.; Ha, S.; Haan, J. L. *Electrochimica Acta* **2014**, *137*, 654.

(55) Qiao, J.; Liu, Y.; Hong, F.; Zhang, J. *Chemical Society Reviews* **2014**, *43*, 631.

(56) Amatore, C.; Saveant, J. M. *Journal of the American Chemical Society* **1981**, *103*, 5021.

(57) Bandi, A. *Journal of The Electrochemical Society* **1990**, *137*, 2157.

(58) Ogura, K.; Yoshida, I. *Journal of Molecular Catalysis* **1988**, *47*, 51.

(59) Portenkirchner, E.; Oppelt, K.; Ulbricht, C.; Egbe, D. A. M.; Neugebauer, H.; Knör, G.; Sariciftci, N. S. *Journal of Organometallic Chemistry* **2012**, *716*, 19.

(60) Lim, R. J.; Xie, M.; Sk, M. A.; Lee, J.-M.; Fisher, A.; Wang, X.; Lim, K. H. *Catalysis Today* **2014**, *233*, 169.

(61) Hori, Y.; Kikuchi, K.; Murata, A.; Suzuki, S. *Chemistry Letters* **1986**, *15*, 897.

(62) Li, C. W.; Kanan, M. W. *Journal of the American Chemical Society* **2012**, *134*, 7231.

(63) Ohkawa, K.; Hashimoto, K.; Fujishima, A.; Noguchi, Y.; Nakayama, S. *Journal of Electroanalytical Chemistry* **1993**, *345*, 445.

(64) Ohkawa, K.; Noguchi, Y.; Nakayama, S.; Hashimoto, K.; Fujishima, A. *Journal of Electroanalytical Chemistry* **1993**, *348*, 459.

(65) Ohkawa, K.; Noguchi, Y.; Nakayama, S.; Hashimoto, K.; Fujishima, A. *Journal of Electroanalytical Chemistry* **1994**, *367*, 165.

(66) Kolbe, D.; Vielstich, W. *Electrochimica Acta* **1996**, *41*, 2457.

(67) Hoshi, N.; Noma, M.; Suzuki, T.; Hori, Y. *Journal of Electroanalytical Chemistry* **1997**, *421*, 15.

2. Synthesis and Characterization of Palladium and Palladium-Copper Alloyed Nanostructures

2.1 Introduction

Pd is a very important element in many applications such as hydrogen storage[1] and the use as catalysts for reactions.[2,3] Among them, Pd and its alloys are particularly attractive for the use as electrocatalysts in fuel cell applications. Due to its similarity to Pt in both atomic size and crystal structure, Pd is a potential alternative to Pt as a fuel cell electrocatalyst at reduced cost.[4] More importantly, Pd, unlike Pt, is able to resist CO poisoning to some degree, which shows better performance than Pt in formic acid oxidation.[5,6]

In the past decade, more and more attention has been paid to controlling sizes and shape of Pd-containing nanoparticles to tailor their catalytic properties.[7] Many chemical routes have been developed to obtain Pd nanostructures *via* either chemical reduction or thermal decomposition of Pd precursors. Most methods were performed in aqueous solution. The size and shape are controlled by a number of factors such as choices of precursors, reducing power of reductants, and additives to the reaction systems. Xia and his co-workers did a series of study on controllable synthesis of Pd nanostructures. Based on their work, the crystallinity of seeds and the growth rates of the nanocrystals to some degree determine the final shapes of nanoparticles.[8] At the initial stage, the Pd seeds formed in two different pathways, namely thermodynamically controlled and kinetically controlled pathways. In thermodynamically controlled pathway, shapes of seeds are primarily determined by the minimum surface energy. Since the surface energies of different facets of a Pd seed increase in the order of {111}< {100}< {110},[8] seeds tend to form the shapes of single-crystal, single-twinned, or multiple-twinned structure to

minimize the total surface energy. At a very slow reduction rate, the process is controlled by kinetics rather than thermodynamics, resulting in the formation of plate-like seeds with staking faults. The total surface energy of such seeds in kinetically controlled pathway is larger than those controlled by thermodynamics. Additionally, capping ligands and additive ions can affect the growth rates on different facets to control the final shapes of the nanostructures. With the assistance of water-soluble surfactants/polymer (e.g. PVP) and some ions (e.g. citrate, Br^- or Cl^-), shapes and sizes of nanostructures can be controlled very well. For example, PVP prefers to passivate {100} rather than {110} of Pd seeds as well as Ag, leading to slow growth rate to form nanocubes.[8] Similar to PVP, halide species such as Br^- can also strongly bond to the facets {100} of Pd nanocrystals during the growth, which leads to formation of nanocubes.[7] The presence of Br^- ions favors to control sizes of Pd nanocubes,[3] due to retardation of reduction kinetics by formation complexes with Pd^{2+}.[7] In addition to Br^-, I^- has also been reported to favor in the formation of nanocubes.[9] In contrast to PVP and Br^-, citrate ions preferably adsorb on {111} facets of Pd nanostructures, resulting in the formation of octahedrons and icosahedrons.[8] Xiong *et al*. in the presence of bromide ions, by adjusting amounts of ethylene glycol (EG) in the mixture grew Pd nanocubes to nanorods and nanobars, the formation mechanism of which was attributed to oxidative etching on specific facets of nanocubes. More recently, more complex polyhedra have been demonstrated by seeded growth method using seeds with simple shapes enclosed by low index facets such as cubes or spheres.[10] Such polyhedra were partially enclosed by high index facets and showed better performance for formic acid oxidation reaction. Though a lot of research attention has been paid on control of morphology of metal particles, exploration of synthesizing small and uniform sizes nanostructures has inspired much research interest, due to high catalytic activities of small nanostructures. Jin *et al*. found out that Pd nanocubes/bars of

6 nm had the lowest maximum CO conversion temperature at 160 ℃, compared to those Pd nanocubes/bars of 10 and 18 nm.[3] This might be caused by the size dependence of turnover frequencies (TOF) that reflected the intrinsic activity of the surface. Based on Gao *et al*'s research results, catalytic activities of Pd nanoparticles on electrolytic CO_2 reduction also exhibited the size dependence from 2.4 to 10.3 nm.[11] Their results showed that Pd of 3.7 nm had the highest CO faradaic efficiency and TOF than the ones of other sizes.

Compared to aqueous synthesis, organic phase synthesis has more choices of reducing agents and ligands, as well as a wide range of reaction temperature from below 0 ℃ to even above 300 ℃. For example, Zheng's group reported to synthesize Pd concave structure in benzyl alcohol.[12] Based on their results, the percentage of (110) facet has a relationship with electrocatalytic activity on formic acid oxidation reaction. Strong coupled Pd tetrahedron/tungsten oxide nanosheet hybrid has also been reported to be synthesized by thermal decomposition of Pd salts and $W(CO)_6$ in the mixture of dimethylformamide and ethanol, recently.[13] This structure exhibited high electrochemical activity and long stability on oxygen reduction reaction due to the change of Pd electronic structure by strongly coupling with tungsten oxide.

To reduce the overall cost of catalysts, attentions have been paid to search for new materials such as alloys to replace pure noble metals. Incorporation of 3-d transition metals such as Cu, Ni, Co, and Fe to form alloys with noble metals, the electronic states of noble metals shift from the original values, and this leads to changes of catalytic behaviors, in some cases, the enhancement of electrochemical activity and CO tolerance in alcohol electro-oxidation reactions.[14,15] Therefore, research has focused on synthesis of Pd-M and Pt-M nanoalloys (M = Cu, Ni, Co, and Fe).[1,16-19]

Among most Pd-M alloy nanostructures, co-reducing Pd and M is a practical method.[20-22] Because of the different reactivity between M and Pd, Pd is usually reduced to form seeds first, and then when the temperature increase high enough, the more active metal can be reduced.[23] Additionally, by increasing the concentrations of reducing agent--formanilide, a series of morphologies of Pd-Cu nanostructures, such as cubes, truncated cubes, cuboctahedra, could be obtained by co-reduced $Pd(acac)_2$ and $Cu(acac)_2$.[24] Increasing concentrations of reductant was conductive to the growth of Cu and Pd along <111> direction. Interconnected, three-dimensional Pd-Cu nanowire networks has been reported by using a one-step colloidal method, in which $Pd(acac)_2$ and $CuSO_4 \cdot 5H_2O$ were co-reduced by ethylene glycol at 200 ℃ in the presence of poly(vinylpyrrolidone) (PVP).[25] In a similar synthetic system without PVP, Hu *et al.* applied solventhermal method to obtain additive-free spherical hollow palladium-copper supported on multiwalled carbon nanotubes.[26] On the other hand, galvanic process has been used by injecting Pd precursor into Cu particle solution to form hollow structures.[27] To obtain monodisperse PdM nanoalloys, Ho and its coworkers developed a facile route, in which metal acetylacetonate, $M(acac)_2$ (M= Cu or Co) and $Pd(acac)_2$ were co-reduced by t-butylamine in oleylamine and 1-octadecene (ODE).[28] The average size of the Pd-Cu particles is as small as 3.5 nm.

The organic phase synthesis has advantages to prepare uniform, ultrafine nanoparticles which are potentially more active in catalytic reactions due to the high surface to volume ratio. In this work, we develop a new one-pot, co-reduction method to synthesize Pd and Pd-Cu nanoparticles. By using different reducing agents, we obtained Pd and Pd-Cu nanostructures with different morphologies and sizes at relatively low synthetic temperatures. Compared to samples synthesized by L-ascorbyl-6-palmitate, the ones synthesized by phenylphosphinic acid displayed

smaller and uniform sizes. We also found that the reducing agents function to determine the ratio of Cu/Pd in the nanoalloys.

2.2. Experimental Details

2.2.1 Chemicals and Materials

Pd 2,4-pentanedionate ($Pd(acac)_2$), copper 2,4-pentanedionate ($Cu(acac)_2$, 98%), copper chloride ($CuCl_2$, anhydrous), L-ascorbyl-6-palmitate (99%), dibenzyl ether and hexadecylamine (HDA) were purchased from Alfa Aesar Company. Phenylphosphinic acid was purcheasd from Sigma Aldrich. High purity reagents HCl (99.999%,) and HNO_3 (99.999%,) for ICP-MS were purchased from Alfa Aesar Company. All chemicals were used as received without further purification.

2.2.2 Instrumentation

TEM images were acquired by a JEOL 100 CX electron microscope at 100 kV acceleration voltages. The samples for TEM were deposited on Cu grids and dried in the air. A Rigaku MiniFlex X-ray diffractometer with Cu $K\alpha$ radiation ($\lambda = 1.541$ Å) was applied to obtain PXRD patterns of samples. The elemental concentration of the samples was obtained by Thermo Scientific iCAP Q inductively coupled plasma mass spectrometer. The samples were prepared by dissolving in aqua regia composed of HCl (99.999%,) and HNO_3 (99.999%,) with volume ratio 3/1 and then diluting with 2% HNO_3 matrix.

2.2.3 Synthesis of Pd Nanostructures

Pd nanostructures were synthesized by reducing Pd precursors in the organic phase using L-ascorbyl-6-palmitate or phenylphosphinic acid as reducing agents listed in Table 2-1. In a typical synthetic method, 5 mL benzyl ether was used to dissolve $Pd(acac)_2$ (25 mg or 0.082 mM), HDA (0.4 g), and certain amounts of reducing agents (shown in Table 2-1) in a 50 mL

three-neck round bottom flask equipped with a magnetic stir bar. After degasing the reaction mixture for ~20 min at room temperature, the reaction was heated up to 120 ℃. The color of the reaction solution changed to yellow when temperature was below around 60℃, to colorless from and orange. When the temperature reached close to 100 ℃, the clear orange solution turned opaque black, indicating the formation of Pd seeds. The mixture was maintained at 120 ℃ for another 20 minutes. The product was initially precipitated by centrifugation with a mixture of toluene and methanol (v/v 1:1) at 6,000 rpm. The precipitate was then purified by a mixture of toluene and methanol (v/v 1:2). The final product was dispersed in toluene.

2.2.4 Synthesis of Palladium-Copper Nanostructures

Pd-Cu alloyed nanostructures were synthesized by co-reducing the Pd and Cu precursors in the organic phases using reducing agents L-ascorbyl-6-palmitate or phenylphosphinic acid as reducing agents listed in Table 2-1. In a typical synthetic method, 5 mL dibenzyl ether was used to dissolve $Pd(acac)_2$ (25 mg or 0.082 mM) and HDA (0.4 g) in a 50 mL three-neck round bottom flask equipped with a magnetic stir bar. Copper precursors, $CuCl_2$ (40 mg or 0.297 mM), or $Cu(acac)_2$ (79 mg or 0.299 mM),and reducing agents (shown in Table 2-1) were then added to the flask. After degasing the reaction mixture for ~20 min at room temperature, the reaction was heated up to 120 ℃. The color of the reaction solution changed rapidly from yellow, to colorless and orange with temperature increasing from 50 ℃ to about 85 ℃. When the temperature reached close to 100 ℃, the clear orange solution turned opaque black, indicating the formation of Pd seeds. The temperature was then raised to 180℃ and kept for another 20 min to further reduce the Cu precursor. The product was initially precipitated by centrifugation. Briefly, when the temperature reduced to 130 ℃, the reaction solution was removed from the flask and distributed into two 15 mL centrifuge tubes filled with 12 mL mixture of toluene and methanol

(v/v 1:1), and then centrifuged at 6,000 rpm for 4 mins. Samples were then redispersed in 7.5 mL mixture of toluene and methanol (v/v 1:2), and centrifuged at 6,000 rpm for 4 mins. 2-1 is the summary of the synthesis of Pd and Pd-Cu nanostructures, in which precursors, solvents and reducing agents are listed.

Table 2-1. Summary of experimental parameters for synthesis of Pd and Pd-Cu nanostructures

Sample name	Pd precursor	Copper precursor	Ligands	Solvent	Reducing agent
Pd-Cu(A)	$Pd(acac)_2$	$CuCl_2$	HDA	benzyl ether	0.18 g L-asorbic-6-palmitate
Pd(A)	$Pd(acac)_2$	-	HDA	benzyl ether	0.18 g L-asorbic-6-palmitate
Pd-Cu(B)	$Pd(acac)_2$	$CuCl_2$	HDA	benzyl ether	0.062 g phenylphosphinic acid
Pd(B)	$Pd(acac)_2$	-	HDA	benzyl ether	0.062 g phenylphosphinic acid
Pd-Cu(C)	$Pd(acac)_2$	$Cu(acac)_2$	HDA	benzyl ether	0.18 g L-asorbic-6-palmitate
Pd-Cu(D)	$Pd(acac)_2$	$Cu(acac)_2$	HDA	benzyl ether	0.062 g phenylphosphinic acid

2.3 Results and Discussion

The commonly-used strategy for synthesis of Pd particles is to reduce Pd precursors, such as $PdCl_2$, Na_2PdCl_4, and $Pd(acac)_2$.[3,23,29,30] Because Pd precursors are usually strong oxidizers, Pd particles can form using amine as reducing agent at relatively low temperatures such as 160 ℃.[23] Another common method is to reduce Pd precursors with reducing agents, such as 1,2-hexadecanediol.[18] The strategy to synthesize Pd-Cu nanoalloy is usually a two-step method shown in Figure 2-5. In the first step, Pd precursors are reduced to small particles, and then when

the temperature was increased to 180 ℃, copper complex is reduced, during the process of which copper is assumed to incorporate into Pd lattices.

In this study, we chose phenylphosphinic acid and L-ascorbyl-6-palmitate, the structures of which are displayed below in Figure 2-1, to serve as reducing agents. Compared to traditional reducing agents such 1,2-hexadecanediol or amines, these two oily strong reducing agents may form Pd seeds at around 100 ℃. Synthesis at such a low temperature is believed to be helpful to control sizes of nanoparticles.

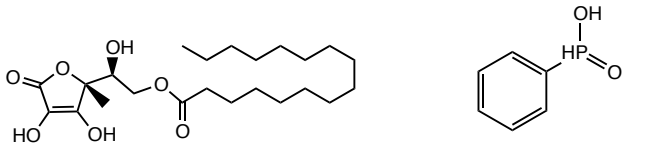

L-ascorbyl-6-palmitate Phenylphosphinic Acid

Figure 2-1. Structures of reducing agents, L-ascorbyl-6-palmitate and phenylphosphinic acid.

2.3.1 Pd Nanostructures

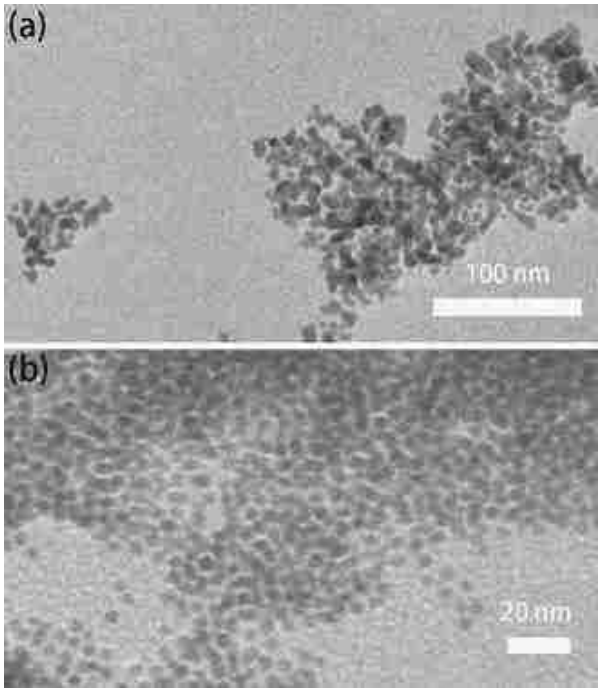

Figure 2-2. TEM images of Pd nanostructures synthesized using different reducing agents: (a) L-ascorbyl-6-palmitate, and (b) phenylphosphinic acid.

Pd nanostructures were synthesized by reducing Pd precursors in the organic phase using L-ascorbyl-6-palmitate or phenylphosphinic acid as reducing agents. Figure 2-2 shows the TEM images of Pd nanostructures synthesized by the two reducing agents. The particles synthesized by phenylphosphinic acid appeared to be spherical shape with an average size of 4.15 nm (Figure 2-2b). In contrast to phenylphosphinic acid, the reaction used L-ascorbyl-6-palmitate as reducing agent tends to form irregular branched structures with branch size of 10.52 nm (Figure 2-2a). In addition, the sizes of the Pd nanostructures synthesized by phenylphosphinic acid are smaller than those synthesized by L-ascorbyl-6-palmitate.

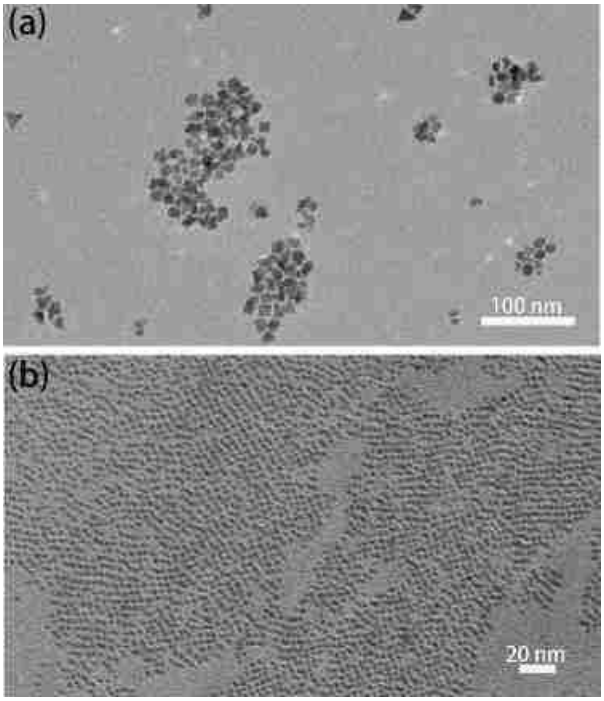

Figure 2-3. TEM images of Pd seeds taken from the aliquot samples in the synthesis using different reducing agents: (a) L-ascorbyl-6-palmitate, (b) phenylphosphinic acid.

To better understand the growth process, aliquot samples were taken from each reaction when the temperature reached 120 ^{o}C and the Pd seeds formed. The morphologies of Pd seeds

synthesized under different conditions are displayed in TEM images of Figure 2-3. The average size of the Pd seeds synthesized by L-ascorbyl-6- palmitate is 9.88 nm, much larger than those synthesized by phenylphosphinic acid (an average size of 2.13 nm). This result is in agreed with observation of Pd particles in Figure 2-1, suggesting that the size and shape of the Pd nanoparticles could be tuned by changing the reducing agents. The observation of size difference could be attributed to the reducing power of agents. According to the previous report,[31] the structure of phenylphosphinic acid has two tautomers, forms A and B, in equilibrium, as shown in Figure 2-4. Due to the existence of the lone pair electrons, Form B could serve as a coordinate ligand to Pd ions, thereby slowing down the reduction kinetics of the Pd precursors. In contrast to phenylphosphinic acid, structure of L-ascorbyl-6-palmitate molecules might not coordinate with Pd ions, therefore the reaction performed in fast kinetics.

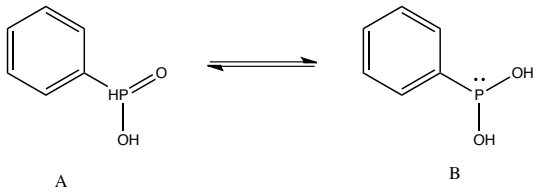

Figure 2-4. Equilibrium between two forms of phenylphosphinic acid tautomers.

2.3.2 Pd-Cu Nanostructures

Pd-Cu nanostructures were synthesized by co-reducing Pd and Cu precursors in the organic phase using L-ascorbyl-6-palmitate or phenylphosphinic acid as reducing agents. To better understand, the effects of reducing agents and precursor reactivity on the formation of bimetallic nanostructures were investigated as illustrated in Figure 2-5. Four samples were synthesized accordingly by using two reducing agents and two Cu precursors. In this case, $Pd(acac)_2$ was used as the Pd precursor in all the reactions. HDA served as a surface ligand of the nanoparticles while L-ascorbyl-6-palmitate and phenylphosphinic acid were the reducing agents.

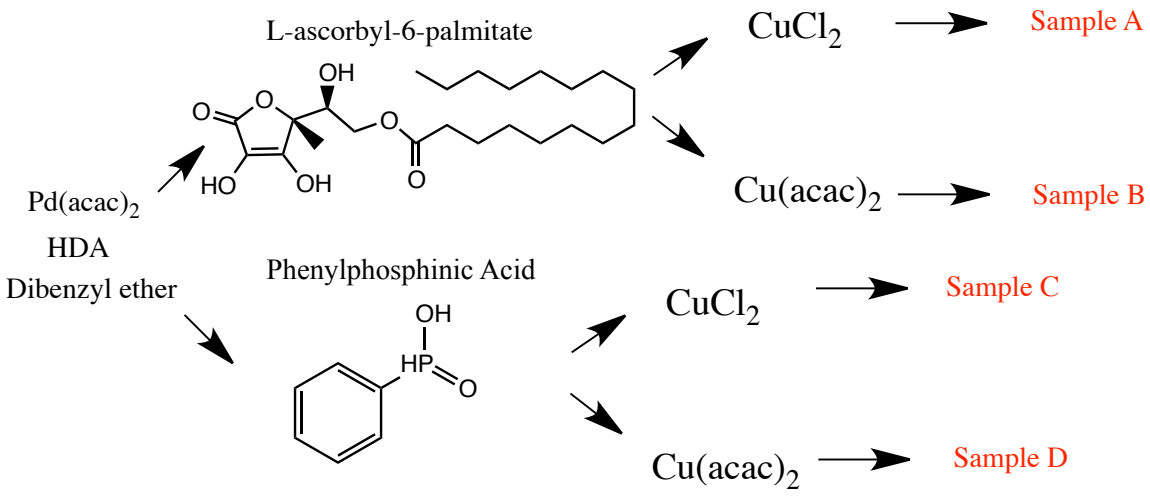

Figure 2-5. Schematic illustration of Pd-Cu nanostructure synthesis

Compared to Pd precursors, Cu precursors have lower standard redox potentials; therefore the reduction temperature for Cu is expected to be higher than that for Pd. According to the previous report,[23] Cu precursors (e.g., $CuCl_2$ and $Cu(acac)_2$)can be reduced at ~180 ℃ or above using amines as reducing agents. Figure 2-6 illustrates the process of the co-reduction. Due to the difference in the redox potential, Pd is anticipated to form at the early stage of the reaction at ~100 ^{o}C before Cu precursor is reduced at higher temperature. A Pd@Cu core-shell structure is expected to form initially and turn into Pd-Cu alloy through diffusion at high temperature.

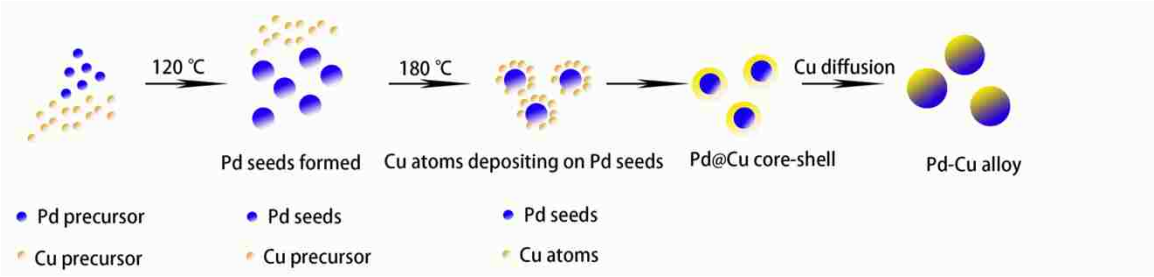

Figure 2-6. Schematic illustration of the Pd-Cu alloyed nanostructure formation.

Figure 2-7 displays the TEM images of Pu-Cu particles. The average sizes of nanoparticles are 22.6 nm 4.51 nm, 5.86 nm, and 3.27 nm for samples Pd-Cu(A), Pd-Cu(B), Pd-Cu(C), and Pd-Cu(D), respectively. Compared to the others, the reaction used $CuCl_2$ as

precursors yielded nanoparticles with large average size. This observation could be attributed to the low redox potential of CuCl, leading to a lower rate of Cu formation. The slower reduction kinetics results in less seeds and thus larger particles during the growth process. [32] This result was in agreement with the previous reports in the aqueous synthetic environment.[33] Similar to that of Pd, reduction used phenylphosphinic acid generated smaller particles as compared to that used L-ascorbyl-6-palmitate.

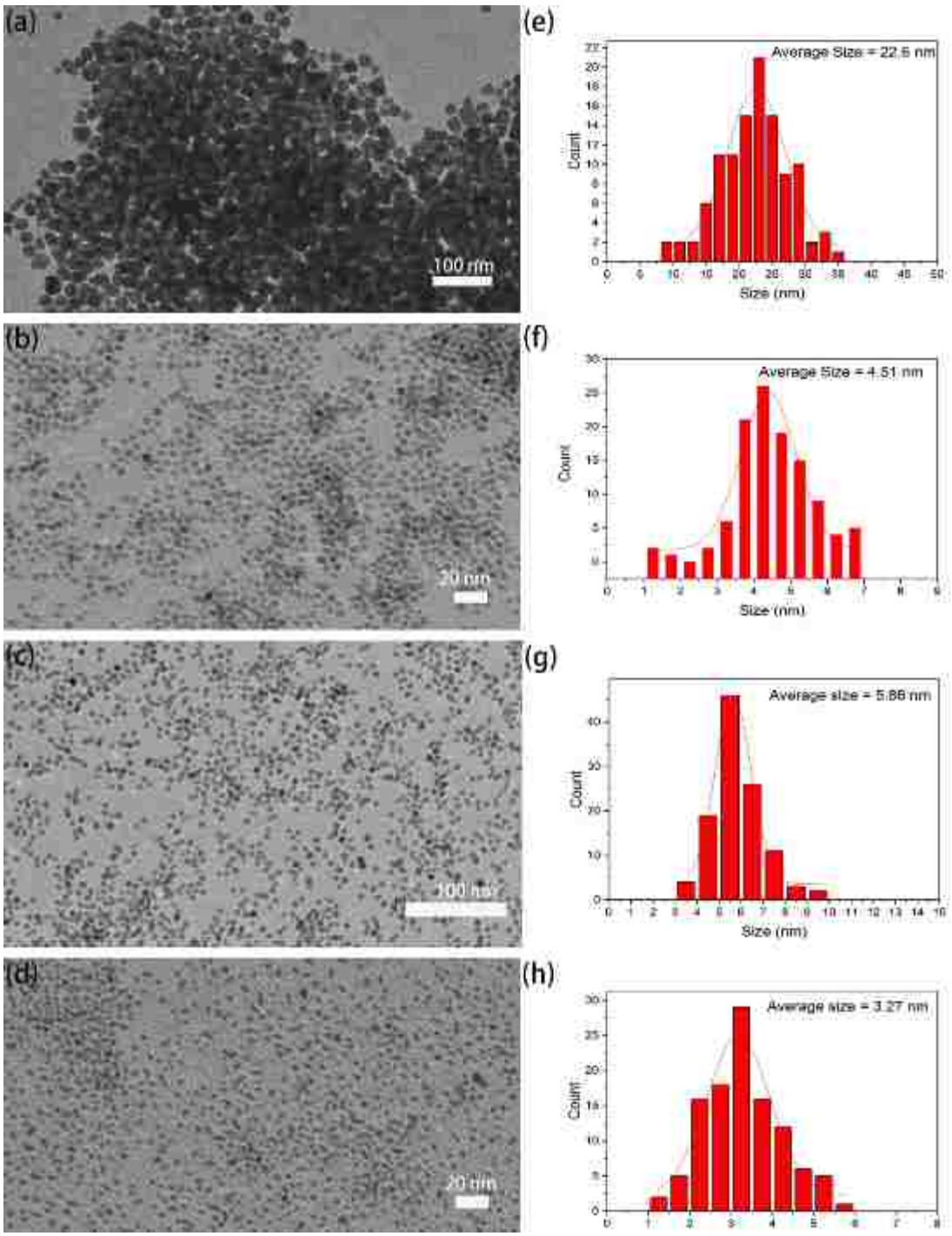

Figure 2-7. TEM images of Pd-Cu nanostructures synthesized under different conditions corresponding to the samples: (a) Pd-Cu(A); (b)Pd-Cu(B); (c) Pd-Cu(C); and (d) Pd-Cu(D). (e-h) histograms of particle size distribution of corresponding samples in (a-d).

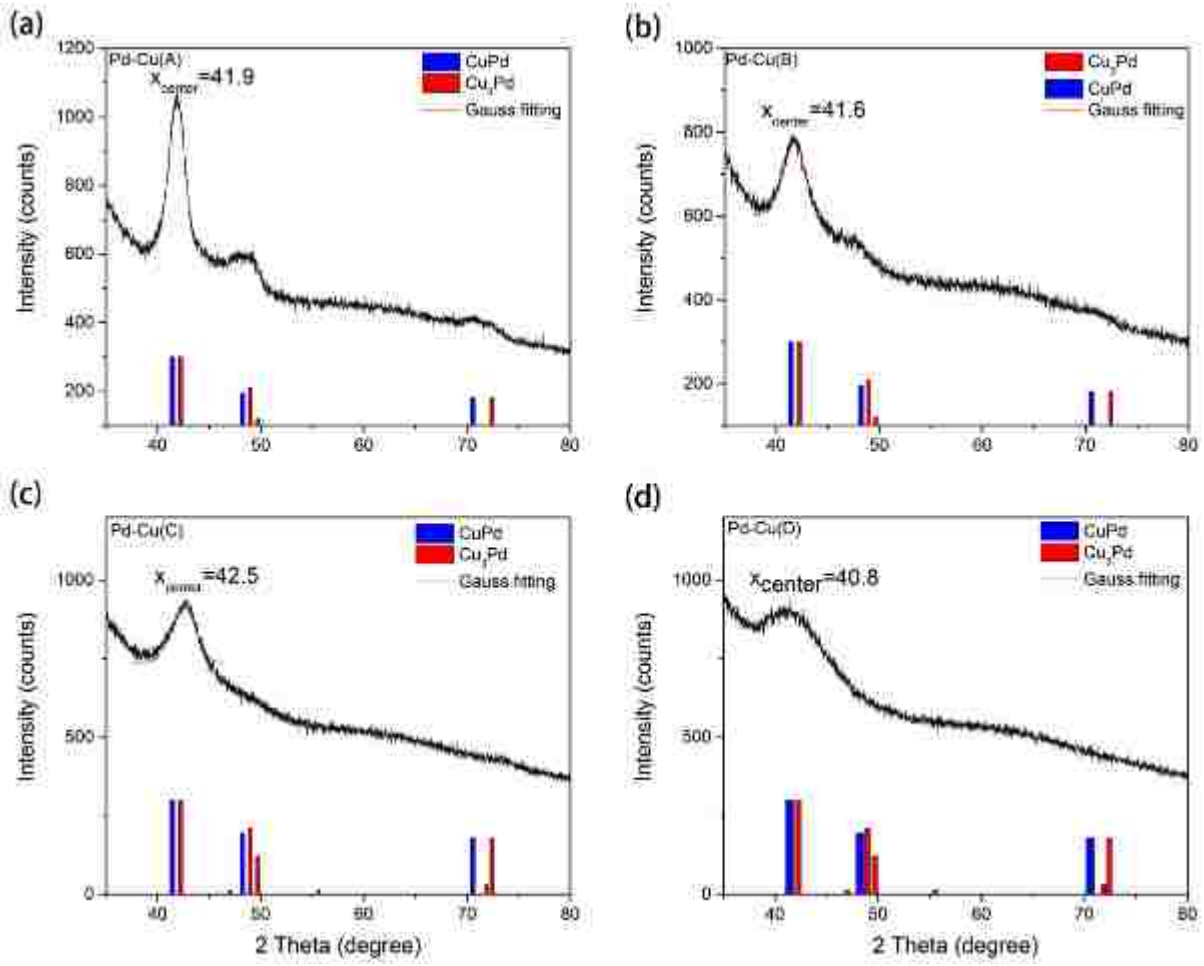

Figure 2-8. PXRD patterns of Pd-Cu nanostructures at a scan rate 0.02°/min from 10° to 90° with Cu $K\alpha$ radiation ($\lambda = 1.541$ Å)*: (a) Pd-Cu(A); (b) Pd-Cu(B); (c) Pd-Cu(C); and (d) Pd-Cu (D).*

The crystal structures of Pd-Cu nanostructures were investigated by XRD (Figure 2-8). The XRD patterns of the samples have a major peak at 40 ~50° which could be assigned to the (111) plane of face-centered cubic structure. The width of the peak becomes broader as the size of sample decreases. The size of the particles can be estimated by the Scherrer formula.

$$L = \frac{K\lambda}{\beta \cos\theta} \qquad (2\text{-}1)$$

where λ is the X-ray wavelength in nanometer (nm), β is full width at half maximum (FWHM) of the diffraction peak, K is a constant related to crystallite shape, normally assumed as 0.9.[34] From equation (2-1), the size of particle (L) is inversely proportional to the FWHM of the peak. By comparing the FWHM of the peak, the sizes of the particles decreased in the order of Pd-Cu(A) > Pd-Cu(C) > Pd-Cu(B) > Pd-Cu(D). This trend agrees with the size distribution results obtained from the TEM images.

Theoretically, the d-spacing of a crystal structure can be determined by the Bragg's law based on the XRD results and equation (2-2).

$$d = \frac{\lambda}{2\sin\theta} \qquad (2\text{-}2)$$

where λ is wavelength of incident light and theta is scattering angle. Since Pd-Cu is cubic crystal structure, d can also be expressed by equation (2-3).

$$d = \frac{a}{\sqrt{h^2+k^2+l^2}} \qquad (2\text{-}3)$$

where *a* is lattice constant, and *h,k,l* are Miller indices of a specific crystal plane. The lattice constant of a sample can then be derived from d values and their corresponding crystal planes. Based on equations (2-2) and (2-3), the d values and lattice constant *a* of the samples are calculated and listed in Table 2-2. The lattice constant of the alloyed nanoparticles is located between those of Pd and Cu. Using the Vegard's law, the composition can be calculated assuming linear mixing.[18]

$$a_{PdCu} = xa_{Pd} + (1-x)a_{Cu} \qquad (2\text{-}4)$$

where a_{PdCu}, a_{Cu}, and a_{Pd} are the lattice constants of Pd-Cu alloy, Cu, and Pd, respectively. The percentage of Pd (x) in each alloyed sample can be derived and the results were listed in Table 2-3. The composition was also examined by elemental analysis using ICP-MS and the

results were listed in Table 2-4. The discrepancy could be attributed to the simple assumption made in the Vegard's law without consideration several physical factors such as relative atomic sizes of the elements, relative volume per valence electron in crystal of pure elements, Brillouin-zone effects.[35] Therefore, ICP-MS measurement provides more accurate results for the composition of the samples.

Table 2-2 d-spacing and lattice constants calculated from the peak assigned to (111) plane of the face-centered cubic structure in PXRD pattern for each sample.

	2θ of Peak (°)	*d* value (nm)	*a* value (nm)
Pd-Cu(A)	41.96	0.2154	0.3730
Pd-Cu(B)	41.6	0.2168	0.3756
Pd-Cu(C)	42.66	0.2116	0.3666
Pd-Cu(D)	40.75	0.2212	0.3831

Table 2-3 Percentage of Pd and Cu for each sample calculated by the Vegards' Law.

	2θ of Peak (°)	*a* value (nm)	*Pd %* (a_{Pd}=0.389 nm)	*Cu %* (a_{Cu}=0.360 nm)
Pd-Cu(A)	41.9	0.3158	44.6%	55.4%
Pd-Cu(B)	41.6	0.3756	53.5%	46.5%
Pd-Cu(C)	42.7	0.3666	22.7%	77.3%
Pd-Cu(D)	40.8	0.3831	79.4%	20.6%

Table 2-4. Percentage of Pd and Cu for each sample measured by ICP-MS.

	Pd Atom%	Cu Atom%
Pd-Cu(A)	38%	62%
Pd-Cu(B)	38.4%	61.6 %
Pd-Cu(C)	22%	78%
Pd-Cu(D)	26.4%	73.6%

2.4 Conclusion

Different sizes and shapes of Pd nanostructures were successfully synthesized by using the two reducing agents (i.e., L-ascorbyl-6-palmitate or phenylphosphinic acid). Pd nanostructures synthesized by L-ascorbyl-6-palmitate trended to exhibit irregular branch shapes or rod like shapes in large sizes. In contrast, phenylphosphinic acid favored to form spherical and uniform sizes Pd nanostructures. The average sizes of Pd nanostructures synthesized by L-ascorbyl-6-palmitate were larger than those by phenylphosphinic acid. To better understand the effect of reducing agents on sizes of particles, we did investigate the Pd seeds before they grew up to nanocrystals. The size statistics of Pd seeds further demonstrated phenylphosphinic acid could control the size of Pd nanoparticles. However, the detailed mechanism is still unclear.

Different sizes and shapes of Pd-Cu nanostructures were successfully synthesized by using the two reducing agents (i.e., L-ascorbyl-6-palmitate or phenylphosphinic acid) and two Cu precursors (i.e. $CuCl_2$ and $Cu(acac)_2$). Based on our result, the process of Pd-Cu formation is thought to follow a two-step reaction. The Pd precursor was initially reduced to form Pd seed, followed by the growth of Pd-Cu final nanostructures. While phenylphosphinic acid is a suitable reducing agent to form small and uniform spherical nanoparticles, L-ascorbyl-6-palmitate tends

to form particles with irregular morphology. Furthermore, we also found that the reducing agents play important roles to control the composition of alloys. The ICP-MS results showed that at a fixed Pd/Cu ratio phenylphosphinic acid favored to increase the percentage of Cu in Pd-Cu system. By manipulating the reducing agents, different nanostructures can be obtained and further investigation of mechanisms is required to understand the crystal growth.

2.5 References

(1) Higuchi, K.; Yamamoto, K.; Kajioka, H.; Toiyama, K.; Honda, M.; Orimo, S.; Fujii, H. *Journal of Alloys and Compounds* **2002**, *330–332*, 526.

(2) Kolmakov, A.; Klenov, D. O.; Lilach, Y.; Stemmer, S.; Moskovits, M. *Nano Letters* **2005**, *5*, 667.

(3) Jin, M.; Liu, H.; Zhang, H.; Xie, Z.; Liu, J.; Xia, Y. *Nano Res.* **2011**, *4*, 83.

(4) Antolini, E. *Energy & Environmental Science* **2009**, *2*, 915.

(5) Babu, P. K.; Kim, H. S.; Chung, J. H.; Oldfield, E.; Wieckowski, A. *The Journal of Physical Chemistry B* **2004**, *108*, 20228.

(6) Arenz, M.; Stamenkovic, V.; Schmidt, T. J.; Wandelt, K.; Ross, P. N.; Markovic, N. M. *Physical Chemistry Chemical Physics* **2003**, *5*, 4242.

(7) Zhang, H.; Jin, M.; Xiong, Y.; Lim, B.; Xia, Y. *Accounts of Chemical Research* **2013**, *46*, 1783.

(8) Xiong, Y.; Xia, Y. *Advanced Materials* **2007**, *19*, 3385.

(9) Niu, W.; Zhang, L.; Xu, G. *ACS Nano* **2010**, *4*, 1987.

(10) Jin, M.; Zhang, H.; Xie, Z.; Xia, Y. *Energy & Environmental Science* **2012**, *5*, 6352.

(11) Gao, D.; Zhou, H.; Wang, J.; Miao, S.; Yang, F.; Wang, G.; Wang, J.; Bao, X. *Journal of the American Chemical Society* **2015**, *137*, 4288.

(12) Huang, X.; Tang, S.; Zhang, H.; Zhou, Z.; Zheng, N. *Journal of the American Chemical Society* **2009**, *131*, 13916.

(13) Lu, Y.; Jiang, Y.; Gao, X.; Wang, X.; Chen, W. *Journal of the American Chemical Society* **2014**, *136*, 11687.

(14) Tang, W.; Zhang, L.; Henkelman, G. *The Journal of Physical Chemistry Letters* **2011**, *2*, 1328.

(15) Park, K.-W.; Choi, J.-H.; Kwon, B.-K.; Lee, S.-A.; Sung, Y.-E.; Ha, H.-Y.; Hong, S.-A.; Kim, H.; Wieckowski, A. *The Journal of Physical Chemistry B* **2002**, *106*, 1869.

(16) Liao, H.; Zhu, J.; Hou, Y. *Nanoscale* **2014**, *6*, 1049.

(17) Guo, S.; Zhang, S.; Sun, X.; Sun, S. *Journal of the American Chemical Society* **2011**, *133*, 15354.

(18) Pires, F. I.; Villullas, H. M. *International Journal of Hydrogen Energy* **2012**, *37*, 17052.

(19) Hu, C.; Cheng, H.; Zhao, Y.; Hu, Y.; Liu, Y.; Dai, L.; Qu, L. *Advanced Materials* **2012**, *24*, 5493.

(20) Xu, C.; Liu, Y.; Wang, J.; Geng, H.; Qiu, H. *Journal of Power Sources* **2012**, *199*, 124.

(21) Xu, C.; Zhang, Y.; Wang, L.; Xu, L.; Bian, X.; Ma, H.; Ding, Y. *Chemistry of Materials* **2009**, *21*, 3110.

(22) Hosseini, H.; Mahyari, M.; Bagheri, A.; Shaabani, A. *Journal of Power Sources* **2014**, *247*, 70.

(23) Chen, S.; Jenkins, S. V.; Tao, J.; Zhu, Y.; Chen, J. *The Journal of Physical Chemistry C* **2013**, *117*, 8924.

(24) Zhang, L.; Hou, F.; Tan, Y. *Chemical Communications* **2012**, *48*, 7152.

(25) Yu, F.; Zhou, W.; Bellabarba, R. M.; Tooze, R. P. *Nanoscale* **2014**, *6*, 1093.

(26) Hu, C.; Guo, Y.; Wang, J.; Yang, L.; Yang, Z.; Bai, Z.; Zhang, J.; Wang, K.; Jiang, K. *ACS Applied Materials & Interfaces* **2012**, *4*, 4461.

(27) Yang, L.; Hu, C.; Wang, J.; Yang, Z.; Guo, Y.; Bai, Z.; Wang, K. *Chemical Communications* **2011**, *47*, 8581.

(28) Ho, S. F.; Mendoza-Garcia, A.; Guo, S.; He, K.; Su, D.; Liu, S.; Metin, O.; Sun, S. *Nanoscale* **2014**, *6*, 6970.

(29) Fu, G.; Han, W.; Yao, L.; Lin, J.; Wei, S.; Chen, Y.; Tang, Y.; Zhou, Y.; Lu, T.; Xia, X. *Journal of Materials Chemistry* **2012**, *22*, 17604.

(30) Yang, J.; Tian, C.; Wang, L.; Fu, H. *Journal of Materials Chemistry* **2011**, *21*, 3384.

(31) Mehrotra, R. N. *Canadian Journal of Chemistry* **1985**, *63*, 663.

(32) Joyce, P. B.; Krzyzewski, T. J.; Bell, G. R.; Jones, T. S.; Malik, S.; Childs, D.; Murray, R. *Physical Review B* **2000**, *62*, 10891.

(33) Zhang, L.; Choi, S.-I.; Tao, J.; Peng, H.-C.; Xie, S.; Zhu, Y.; Xie, Z.; Xia, Y. *Advanced Functional Materials* **2014**, *24*, 7520.

(34) Monshi, A.; Foroughi, M. R.; Monshi, M. R. *World Journal of Nano Science and Engineering* **2012**, *2*, 154.

(35) Denton, A. R.; Ashcroft, N. W. *Physical Review A* **1991**, *43*, 3161.

3. Electrocatalytic Activities of Pd and Pd-Cu Nanostructures for Ethanol Oxidation Reaction

3.1 Introduction

Improving the efficiency of fuel oxidation has attracted considerable attention for direct alcohol fuel cell applications. Compared to methanol and formic acid, ethanol has several advantages such as low toxicity to human, production by fermentation of raw biomass, and high energy density (8.0 kWh/kg) compared to that of methanol (6.1 kW/kg).[1] Most studies focus on ethanol oxidation reaction (EOR) in acidic environment due to widespread use of proton exchange membranes (PEMs) in the commercial fuel cells. Platinum is the most widely used catalytic electrode material. However, because of high cost and low efficiency, scientists are seeking for substitutes of Pt as electrocatalysts for EOR. Palladium-based materials are one of the substitutes of platinum that have been explored.[2-7] Most studies on Pd-based electrocatalysts for EOR were performed in alkaline media.[8] Unlike methanol, the oxidation of ethanol involves cleavage of C-C bond which requires much higher onset potentials to activate the reaction. A few studies have revealed the mechanism of EOR in alkaline solution using Pd electrocatalysts. For example, the mechanism was proposed to have multiple steps as shown in equation (3-1) to (3-4) in a cyclic voltammetry study.[9] It was found that removal of the intermediate (i.e. adsorbed acyl group) by adsorbed hydroxyl group on Pd surface was the rate determining step as shown in equation (3-3). The proposed mechanism indicated that the catalytic rate could be accelerated by increasing concentration of OH^- which was confirmed by performing the EOR in different concentrations of KOH solution.[9]

$$Pd + CH_3CH_2OH \leftrightarrow Pd{-}(CH_3CH_2OH)_{ads}, \quad (3\text{-}1)$$

$$Pd - (CH_3CH_2OH)_{ads} + 3OH^- \rightarrow Pd - (OCCH_3)_{ads} + 3H_2O + 3e^-, \quad (3\text{-}2)$$

$$Pd-(CH_3CO)_{ads}+Pd-OH^-_{ads}\xrightarrow{r.d.s}Pd-CH_3COOH+Pd, \quad (3\text{-}3)$$

$$Pd-CH_3COOH+OH^-\rightarrow Pd+CH_3COO^-+H_2O. \quad (3\text{-}4)$$

Based on DFT calculation, others proposed that the oxidation process involved acetaldehyde formation in the first step and then further oxidation led to the formation of acetate with no evidence of C-C cleavage, as shown in equations (3-5) – (3-7).[10]

$$CH_3CH_2OH+OH^-\rightarrow CH_3CHOH+H_2O \quad (3\text{-}5)$$

$$CH_3CHOH\rightarrow \cdot CH_3CHOH+e \quad (3\text{-}6)$$

$$\cdot\ CH_3CHOH\rightarrow CH_3CHO+\cdot H \quad (3\text{-}7)$$

Similar to the bifunctional mechanism for methanol oxidation,[11] coupling Pd with non-noble metals can enhance catalytic activities and stabilities, as well as reduce the cost in fuel cell applications. Pd-based nanostructures have then been studied electrocatalysts for EOR.[12-18] For example, the Pd-Cu nanocapsules on graphene exhibited electrocatalytic activity 3-fold higher than the commercial Pd/C catalyst.[19] The anodic and cathodic current densities of PdCuPb/C for EOR were 105.3 and 38.8 mA/cm^2, respectively, which were higher than those of commercial Pd/C.[14] More oxygenate species generated on PdCuPb/C surface led to the removal of CO-like poisonous intermediates. In addition, the specific peak current density of 1782 mA/mg$_{Pd}$ was achieved for Pd-Cu catalysts for EOR compared to that of 1060 mA/mg$_{Pd}$ for commercial Pd/C in 0.5 KOH solution.[1] These improvements may benefit from the bifunctional effect which hydroxyl groups strongly attach to the Cu sites while ethanol molecules tightly adsorb on Pd sites, and the mechanism was shown follow in equations (3-8)-(3-13).[20]

$$Pd+CH_3CH_2OH\leftrightarrow Pd-(CH_3CH_2OH)_{ads}, \quad (3\text{-}8)$$

$$Pd-(CH_3CH_2OH)_{ads}+3OH^-\rightarrow Pd-(OCCH_3)_{ads}+3H_2O+3e^-, \quad (3\text{-}9)$$

$$Pd-(CH_3CO)_{ads}+M-OH_{ads}\xrightarrow{r.d.s}Pd-CH_3COOH+M\ (M=Pd/Cu), \quad (3\text{-}10)$$

$$Pd - CH_3COOH + OH^- \rightarrow Pd + CH_3COO^- + H_2O. \quad (3\text{-}11)$$

$$PdCO + Cu(OH)_2 = Pd + Cu + 2H^+ + CO_3^{2-} \quad (3\text{-}12)$$

$$PdHCO + Cu(OH)_2 = Pd + CO_3^{2-} + Cu + 3H^+ + e \quad (3\text{-}13)$$

In this work, we examined the Pd and Pd-Cu nanostructures that were prepared followed the methods in Chapter 2. The structure-property relationship was revealed by comparing the results.

3.2 Experimental Details

3.2.1 Chemicals and Materials

Sodium hydroxide and acetic acid was purchased from Alfa Aesar company. Ethanol were purchased from Koptec. 5% Nafion solution was purchased from Sigma Aldrich. The support carbon black was Vulcan XC 72R. All chemicals were used as received without further purification.

3.2.2 Preparation of Carbon Supported Electrocatalysts.

The nanoparticles were deposited on carbon and treated by acid to remove surfactants using the modified procedures according to the previous reports.[4] The as-synthesized Pd or Pd-Cu samples were mixed with equal mass amount carbon support in 15 mL toluene/acetone v/v 1:1 and sonicated for 1 h. The carbon supported catalysts were separated by centrifuging at 6,000 rpm for 4 min. The precipitates were washed with acetone twice. They were then mixed with 15 mL acetic acid and kept at 65 ℃ overnight. The catalysts were separated by centrifugation and purified twice with water. Finally, the carbon support catalysts were dispersed in water.

3.2.3 Preparation of Working Electrodes

The glassy carbon electrodes with a diameter of 3 mm were polished with 0.05 μm alumina liquid, and sonicated with deionized water. Each sample in water was mixed with 0.05

wt% Nafion in water/ethanol v/v 1:1 to form 1 mg/mL catalyst suspension. Then 10 μL of this solution was dropcasted on the electrode and dried in air.

3.2.4 Assessment of Electrochemical Catalytic Activities

All electrochemical performances were employed on a CHI 760D electrochemical workstation with a three-electrode system. A three-electrode system comprises a working electrode modified with samples, an Ag/AgCl in 1 M KCl reference electrode, and a platinum wire counter electrode. All potentials are converted to reversible hydrogen electrode (RHE), by the equation. $E(RHE) = E(Ag/AgCl) + 0.059pH+0.234$. The electrolytes were the mixture of 0.1 M NaOH solution or 0.1 M NaOH + 1 M ethanol solution, and all solutions were saturated with highly pure nitrogen for 20 min. In cyclic voltammetry (CV) measurement, the potential range was scanned from 0 to 1.4 V vs RHE. Electrochemical active surfaces were determined by the CV method in 0.1 NaOH solutions at a scan rate of 50 mV/s. EOR tests were performed in 0.1 NaOH + 1 M ethanol solutions at the chosen scan rates. The stability tests results were recorded by CV measurement within the range of 0 to 1.4 V at 50 mV/s in 0.1 NaOH + 1 M ethanol solution after 500 cycles. The first cycle data was obtained until the CV curve is stabilized (typically after 5 scans). The i-t curves were measured by chronoamperometry (CA) method at a constant potential of 0.8 V vs RHE in 0.1 NaOH + 1 M Ethanol solutions for 1600s.

3.3 Results and Discussion

3.3.1 Determination of Electrochemical Active Surface Areas

Electrochemical active surface (ECSA) is a very important index to evaluate the catalytic sites of the catalysts. The ECSA can be obtained with CV scanned from 0 to 1.4 V vs RHE. For Pt, the typical method to determine ECSA is to calculate the area of hydrogen adsorption/desorption based on the underpotential deposition (UPD) of hydrogen.[21] This method

is not applicable for Pd because of the interference of hydrogen absorption in Pd.[22-24] Surface oxide reduction, UPD of Cu, and CO stripping are the three commonly used methods to determine the ECSA of Pd.[21,25,26] In the study, we use the reduction charge of surface $Pd(OH)_2$ or Pd-O to determine ECSA of Pd.[27] The CV curves were obtained by sweeping from 0 to 1.4 V vs RHE in 0.1 M NaOH. From CV curves of Pd (Figure 3-1), the region from 0 - 0.37 V is attributed to hydrogen adsorption/desorption. The onset current occurring from ~0.91 V indicates adsorption of hydroxyl group with the loss of two electrons. The adsorbed hydroxyl group further decomposes to Pd-O and H_2O. The mechanism is described in equations (3-14)-(3-16).[9]

$$Pd + OH^- \leftrightarrow Pd{-}OH_{ads} + e^- \quad (3\text{-}14)$$

$$Pd{-}OH_{ads} + OH^- \leftrightarrow Pd{-}O + H_2O + e^- \quad (3\text{-}15)$$

$$Pd{-}OH_{ads} + Pd{-}OH_{ads} \leftrightarrow Pd{-}O + H_2O. \quad (3\text{-}16)$$

In the cathodic sweep, the peak located in the range from 0.6 V ~ 0.7 V was well-defined, suggesting the reduction of $Pd(OH)_2$ or Pd-O to Pd with the gain of two electrons, as shown in equation (3-17).[9]

$$Pd{-}O + H_2O + 2e^- \leftrightarrow Pd + 2OH^-. \quad (3\text{-}17)$$

The peak shifts between the two samples is possibly due to the difference of size and shape. The associated charges (Q_o) of the peak can be used to derive the ECSA based on the equation (3-18) and (3-19).

$$Q_o = 2eN_A\Gamma_O A \quad (3\text{-}18)$$

$$Active\ Surface = \frac{Q_O}{q_O^s} \quad (3\text{-}19)$$

where N_A is Avogadro constant, and Γ_O is the surface concentration of atomic oxygen, which is equal to the density of Pd atom on the surface (N_{Pd}).[26] The charge density for the formation of a fully covered $Pd(OH)_2$ layer (q_O^s) was chosen based on the value reported for typical single-

crystal Pd surface 430[27] $\mu C/cm^2$. The value of Q_o can be calculated by integrating the oxygen desorption peak in alkaline solution. The ECSAs are listed in Table 3-1.

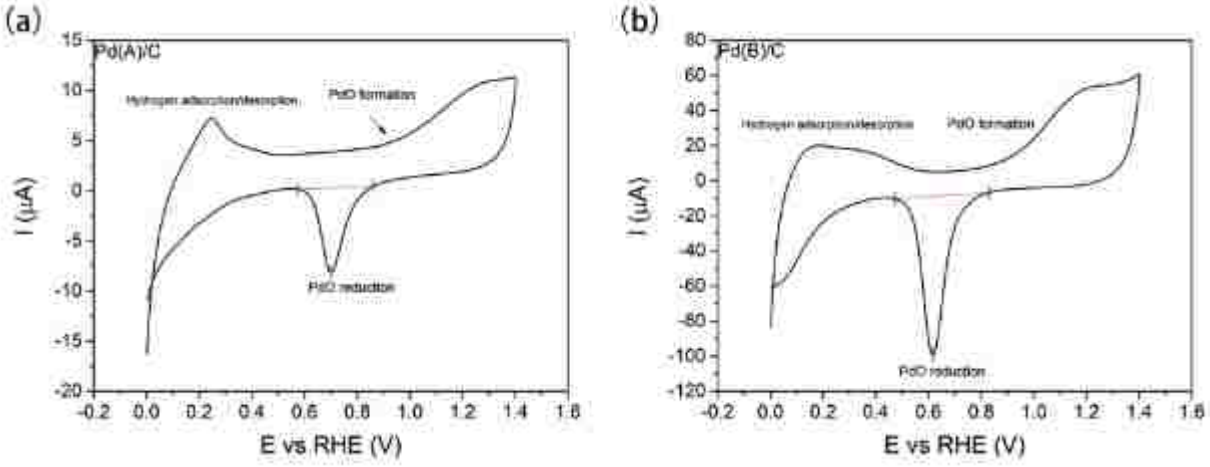

Figure 3-1. CV curves of Pd samples in 0.1 NaOH solution swept from 0 to 1.4 V RHE at a scan rate of 50 mV/s: (a) Pd(A)/C; (b) Pd(B)/C.

Different from the pure Pd samples, the existence of Cu in the alloys shifts the onset oxidation currents appeared at more negative (~ 0.7 V) in Figure 3-2. The alloys typically have smaller overpotentials for Pd oxidation than the pure Pd, which might be due to the presence of Cu on the surface. The mechanism of Pd-O formation for Pd-Cu alloys is described in equations (3-20)-(3-23).[20]

$$Pd + OH^- \leftrightarrow Pd{-}OH_{ads} + e^- \quad (3\text{-}20)$$

$$Pd{-}OH_{ads} + Cu \leftrightarrow Cu\text{-}OH + Pd \quad (3\text{-}21)$$

$$Pd{-}OH_{ads} + OH^- \leftrightarrow Pd{-}O + H_2O + e^- \quad (3\text{-}22)$$

$$Pd{-}OH_{ads} + Pd{-}OH_{ads} \leftrightarrow Pd{-}O + H_2O. \quad (3\text{-}23)$$

It is worth noting that the peak of $Pd(OH)_2$ reduction generally appears around 0.6 – 0.7 V (vs RHE); however, the slight difference of peak position among samples likely depends on the compositions of alloys.

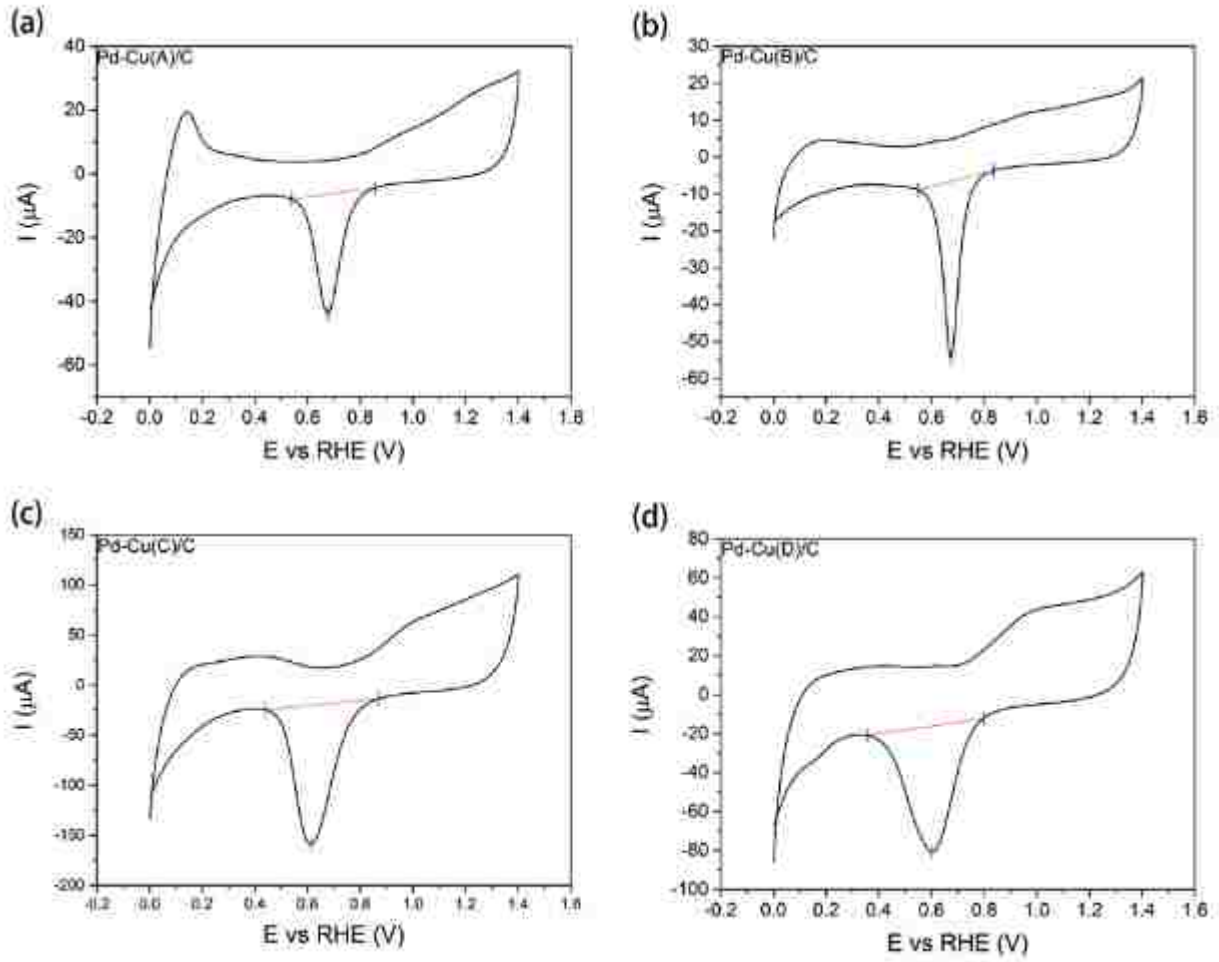

Figure 3-2. CV curves of Pd-Cu/C samples scaned from 0 to 1.4 V vs RHE in 0.1 NaOH solution at 50 mV/s: (a) Pd-Cu(A)/C; (b) is Pd-Cu(B)/C; (c) is Pd-Cu(C)/C; (d) is Pd-Cu(D)/C.

More interestingly, the samples synthesized by the same reducing agent showed similar peak position of Pd-O reduction (Figure 3-3). For example, Pd(A)/C, Pd-Cu(A)/C, and Pd-Cu(B)/C synthesized by using L-ascorbyl-6-palmitate as the reducing agent had PdO reduction peaks at ~0.65 V vs RHE. In contrast, Pd(B)/C, Pd-Cu(C)/C, and Pd-Cu(D)/C synthesized by using phenylphosphinic acid as the reducing agent had lower Pd-O reduction potentials at ~0.610 V.

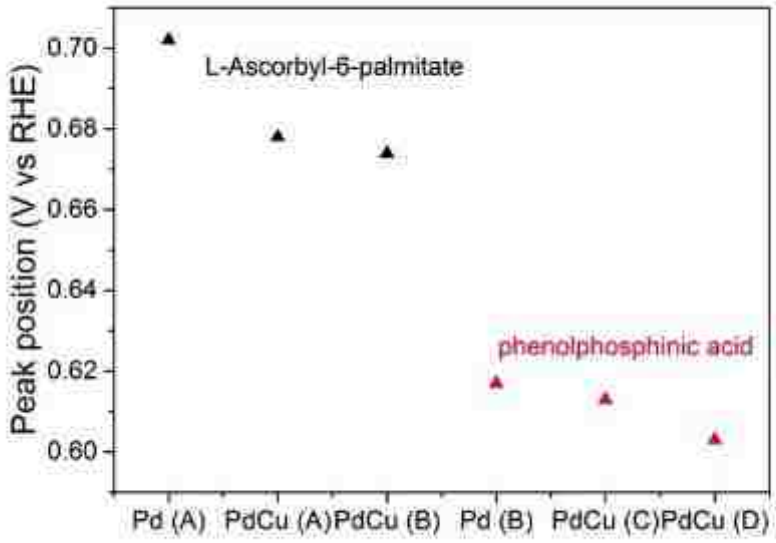

Figure 3-3. Effects of reducing agents on peak position of Pd-O reduction in ethanol oxidation peaks. Solid black triangles represent the samples synthesized by L-ascorbyl-6-palmitate as the reducing agent; solid red triangles represent the samples synthesized by using phenylphosphinic acid as the reducing agent.

To compare the catalytic properties of catalysts, the ECSA and specific electrochemical surface areas (ESA) which are the ECSA normalized by mass of Pd are listed in Table 3-1. According to previous report, the ESA of Pd based electrode are usually under 100 m^2/g_{Pd}.[28] In our case, the Pd samples had the ESA on the order of 10^3 while the ESA of Pd-Cu samples were on the order of 10^4 in Figure 3-4. This large ESA might be the results of the ultrafine particles compared to those in the previous reports; however, we cannot rule out the possibility that the adsorbed oxygen was more than a monolayer in our case because it is lacking a consistent method to determine the upper potential limit[27] for Pd in alkaline solution.

Table 3-1 Summary of electrochemically active surface areas (ECSA) and specific electrochemical surface areas (ESA) of Pd and Pd-Cu nanostrucutures.

Sample	Pd(A)/C	Pd(B)/C	Pd-Cu(A)/C	Pd-Cu(B)/C	Pd-Cu(C)/C	Pd-Cu(D)/C
Pd-O peak V	0.702	0.617	0.678	0.674	0.613	0.603
ECSA cm^2	0.043	0.471	0.206	0.184	1.128	0.619
ESA m^2/g_{Pd}	2151.90	4927.25	2210.92	7611.21	18229.82	15185.43

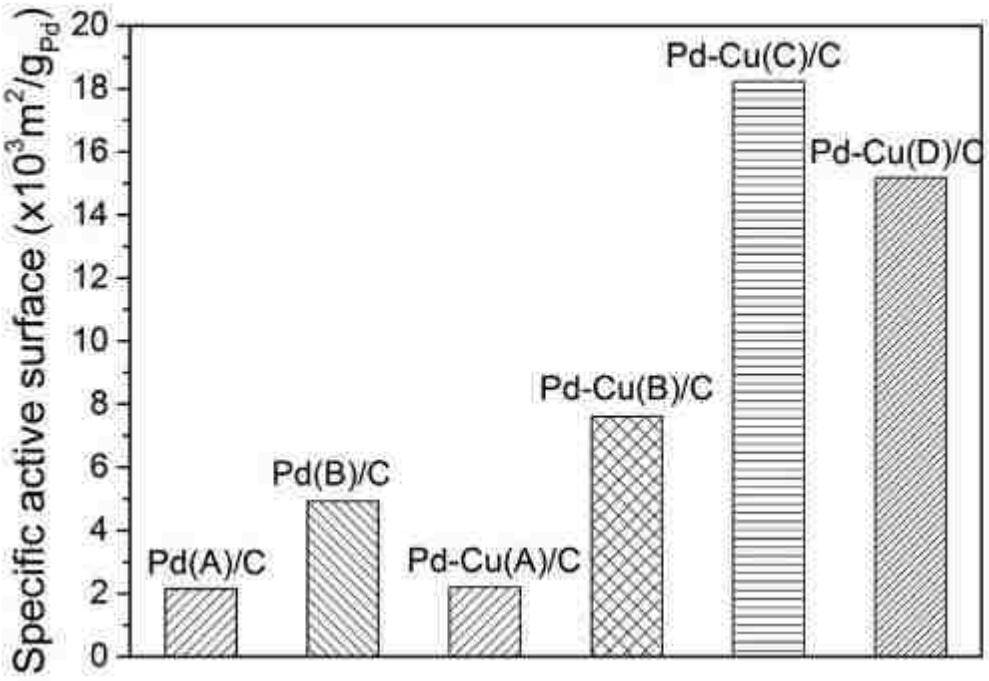

Figure 3-4. Comparison of specific ESA for Pd and Pd-Cu nanostrucutres .

3.3.2 Catalytic Performance of Pd and Pd-Cu Nanostructures on EOR

The electrochemical activities of the Pd and Pd-Cu catalysts were characterized by the CV method in basic solution with ethanol (0.1 M NaOH + 1 M ethanol). Because of the uncertainty of ECSAs of Pd samples, the current were normalized with the mass of Pd loading for comparison. The loading mass of Pd(A)/C, Pd(B)/C, Pd-Cu(A)/C; Pd-Cu(B)/C; Pd-Cu(C)/C;

and Pd-Cu(D)/C are 0.199 μg, 0.955 μg, 0.935 μ, 0.241 μg, 0.619 μg and 0.408 μg, respectively. Figure 3-5 represents the CV curves of pure Pd sameples, Pd(A)/C and Pd(B)/C, in 0.1 NaOH with 1 M ethanol. The peak at region between 0.8 V and 0.9 V were assigned to the oxidation of ethanol. The peak at ~0.6 V as appeared in the cathodic sweep were typically interpreted as one of the two processes: 1) the removal of the oxidation intermediates;[1] and 2) the oxidation of fresh ethanol diffused to the surface of the electrode.[29] We speculated that the latter, oxidation of ethanol, is attributed to this peak at ~0.6 V appeared in the cathodic sweep because the surface of the electrode should be cleaned after the potential reaches 1.4 V vs RHE, suggested that the CO-like intermediates have been oxidized in anodic scan. The peak appeared sharp, indicating that there was probably only one species being oxidized.[28] Pd(A)/C catalyst exhibited lower overpotential (0.797 V) for EOR in the anodic sweep compared to Pd(B)/C (0.852 V). In contrast, Pd(B)/C showed better resistance against CO poisoning, which was estimated by the value of J_f/J_b listed in Table 3-2 (0.866 for Pd(B)/C versus 0.313 for Pd(A)/C). The larger the value of J_f/J_b, the better the resistance against CO poisoning is.

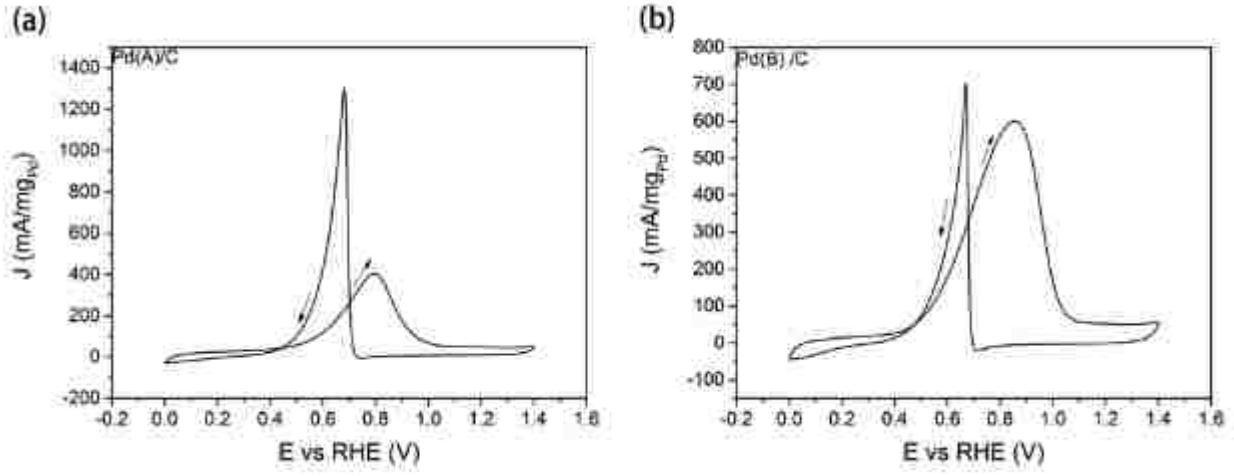

Figure 3-5. Cyclic voltammograms curves of Pd samples in 0.1 NaOH+1 M ethanol from 0 to 1.4 V RHE at a scan of 50 mV/s: (a) Pd(A)/C and (b) Pd(B)/C.

In order to test the tolerance to CO poisoning, i-t measurements have been run in 0.1 NaOH + 1 M ethanol at 0.8 V vs RHE for duration of 1600s (Figure 3-6). The initial currents decreased rapidly to achieve a pseudosteady state.[28] Since CO_{ad} gradually occupied the active sites of surfaces of Pd samples, the currents decayed gradually. Compared to Pd(B)/C, particles of Pd(A)/C have larger sizes resulting in less active Pd exposing to the solution; therefore, the slope of its current density decrease of steady current was larger than that of Pd(B)/C. Pd(B)/C also exhibited higher current density than Pd(A)/C.

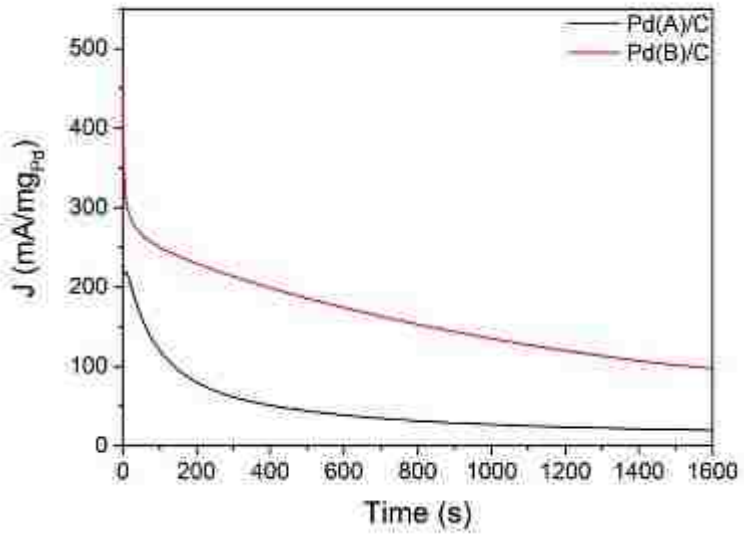

Figure 3-6. i-t curves for Pd(A)/C and Pd(B)/C in 0.1 NaOH + 1 M ethanol at 0.8 V vs RHE. The black curve is for Pd(A)/C and the red curve is for Pd(B)/C.

Catalytic activities of EOR of Pd-Cu nanostructures have been characterized using the same conditions as that for pure Pd nanoparticles, in 0.1 NaOH + 1 M ethanol at a scan rate of 50 mV/s (Figure 3-7). To compare the resistance against CO, the values of J_f/J_b are listed in Table 3-2. Compared to pure Pd samples, Pd-Cu alloys had lower overpotentials and displayed the resistance against CO to some degree due to the introduction of Cu atoms which could change the energy level of d band of Pd.[30]

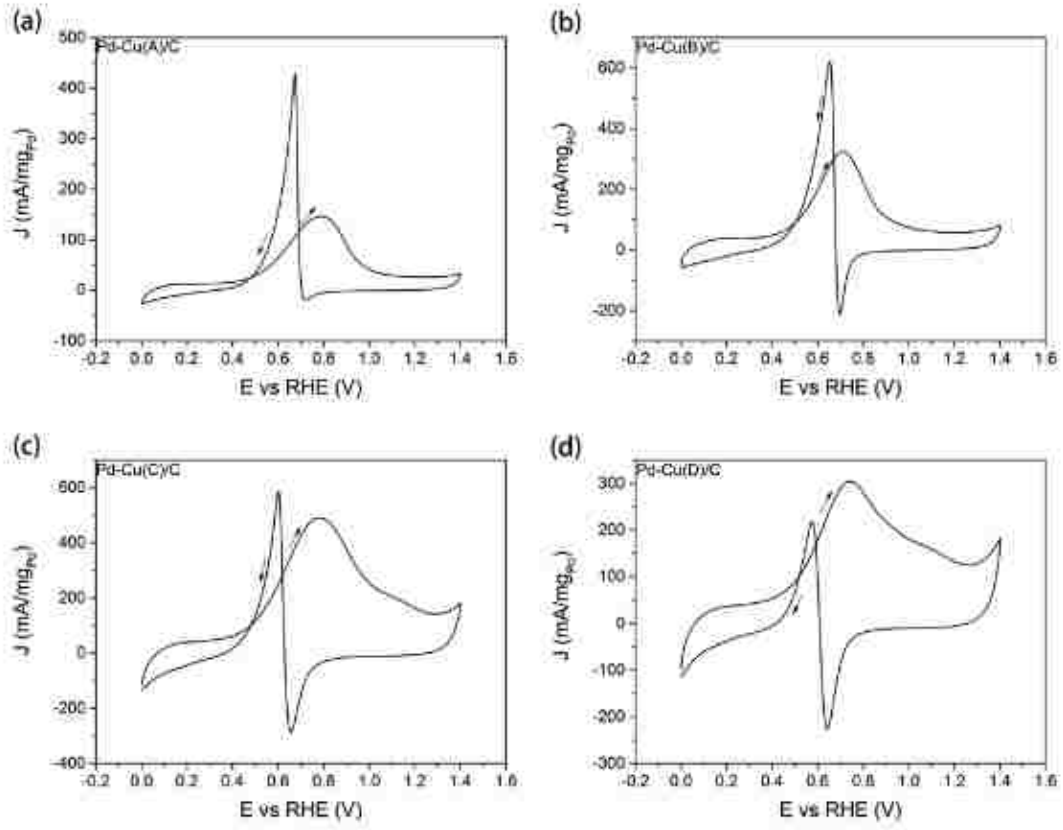

Figure 3-7. CV curves of Pd-Cu/C samples from 0 to 1.4 V RHE in 0.1 NaOH+1 M ethanol at a scan rate of 50 mV/s: (a) Pd-Cu(A)/C; (b) Pd-Cu(B)/C; (c) Pd-Cu(C)/C; and (d) Pd-Cu(D)/C. The curves are normalized by the mass of Pd in each sample.

Table 3-2. Comparison of electrochemical activities of Pd-Cu/C with Pd/C for EOR in 0.1 M NaOH with 1 M Ethanol.

Sample	$E_{p(f)}$ (V)	$J_{p(f)}$ (mA)	$E_{p(b)}$ (V)	$J_{p(b)}$ (mA)	$J_{p(f)}/ J_{p(b)}$
Pd(A)/C	0.794	1.883	0.685	6.016	0.313
Pd(B)/C	0.855	1.223	0.670	1.413	0.866
Pd-Cu(A)/C	0.788	0.660	0.675	1.930	0.342
Pd-Cu(B)/C	0.709	0.433	0.652	0.828	0.523
Pd-Cu(C)/C	0.776	0.269	0.602	0.320	0.841
Pd-Cu(D)/C	0.740	0.200	0.573	0.142	1.408

To understand better the catalytic behaviors of samples for EOR, we compare CV curves at different scan rates from 10 mV/s to 100 mV/s (Figure 3-8). As we know, in CV, the peak current densities of samples increased with the increased scan rates. The values of J_f/J_b are listed in table 3-3. With the increased scan rates, the values of J_f/J_b also increased. At the high potential, Pd has been oxidized to PdO, which blocks adsorption of ethanol on Pd surfaces.[29] Additionally, in the cathodic scan, reducing PdO generate opposite currents to oxidizing ethanol leads to the decrease ethanol oxidation peak. At a high scan rate, more Pd can be oxidized quickly. Therefore, that the anodic peak current densities increase faster than cathodic peak current densities resulting in increase of J_f/J_b, which is against the previous report result.[31]

Table 3-3. Summary of values of J_f/J_b obtained from the CV curves at different scan rates.

Scan rate	Pd(A)	Pd(B)	Pd-Cu(A)	Pd-Cu(B)	Pd-Cu(C)	Pd-Cu(D)
10 mV/s	0.0967	0.322	0.149	0.169	0.478	1.68
30 mV/s	0.19	0.711	0.247	0.361	0.61	1.25
50 mV/s	0.309	0.883	0.349	0.519	0.832	1.42
80 mV/s	0.5	1.056	0.454	0.731	1.041	2.068
100 mV/s	0.501	1.165	0.533	0.838	1.327	2.36

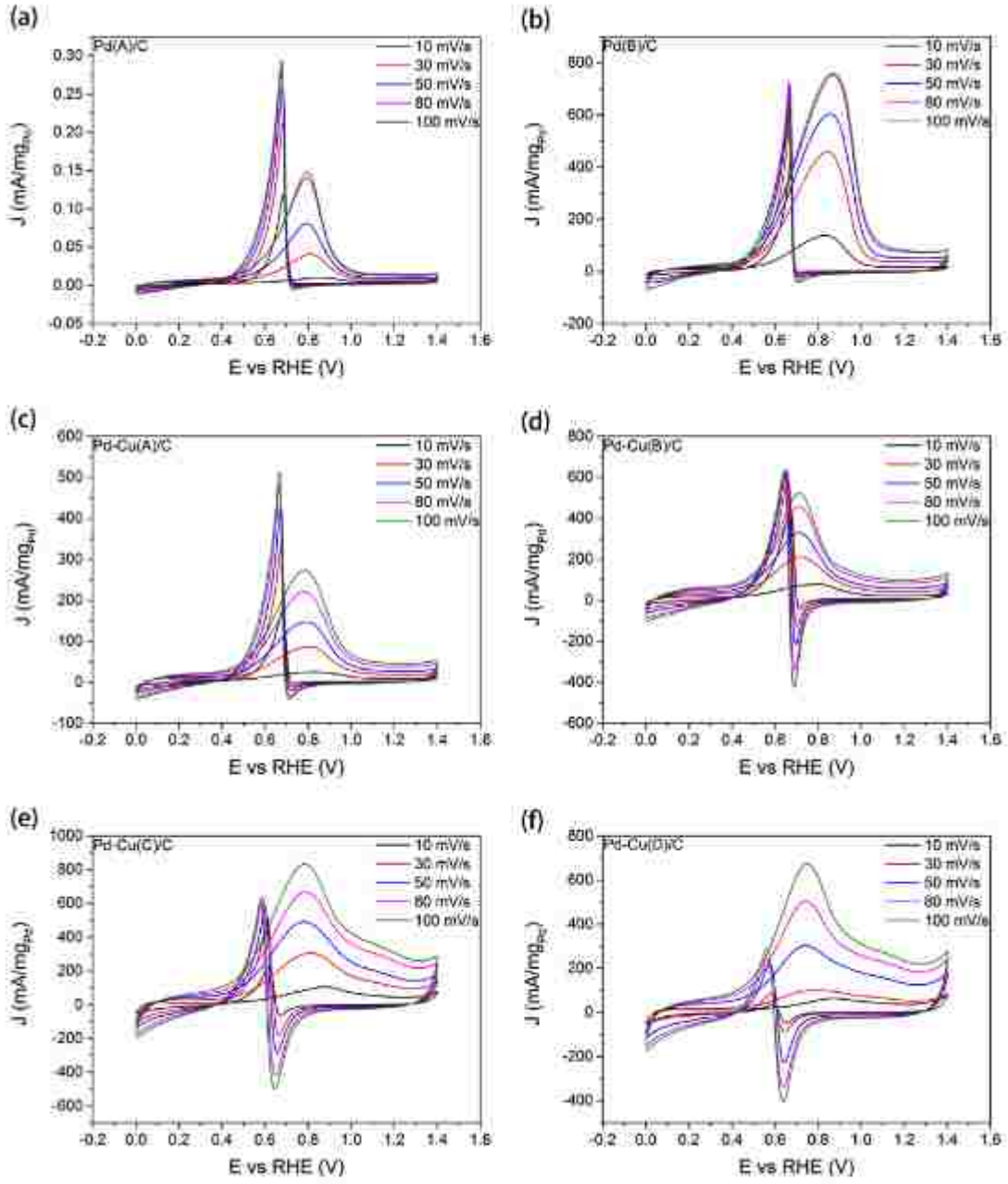

Figure 3-8. CV curves of Pd and Pd-Cu samples in 0.1 NaOH+1 M ethanol from 0 to 1.4 V RHE at different scan rates, 10 mV/s, 30 mV/s, 50 mV/s, 80 mV/s, and 100 mV/s: (a) Pd(A)/C, (b) Pd (B)/C, (c) Pd-Cu(A)/C; (d) Pd-Cu(B)/C; (e) Pd-Cu(C)/C; and (f) Pd-Cu(D)/C. The curves are normalized by mass of Pd in each sample.

The i-t measurement was performed under the same conditions to test the CO tolerance for each catalyst, as shown in Figure 3-9. The EOR on the surfaces of catalysts involves the

adsorption, dehydrogenation and removal of CO-like species.[14] Due to the strong ability to bond with metals, CO-like intermediates can accumulate and occupy the active sites on the surfaces of catalysts. This can result in the very quick decrease of the current densities at the initial stage and reach a steady state. Pd-Cu(B)/C, Pd-Cu(C)/C, and Pd-Cu(D)/C containing smaller particles are more active to resist CO-like intermediates indicating by the slower decrease of current densities than Pd-Cu(A)/C containing larger particles. This result suggested that smaller particles have more active sites for EOR.

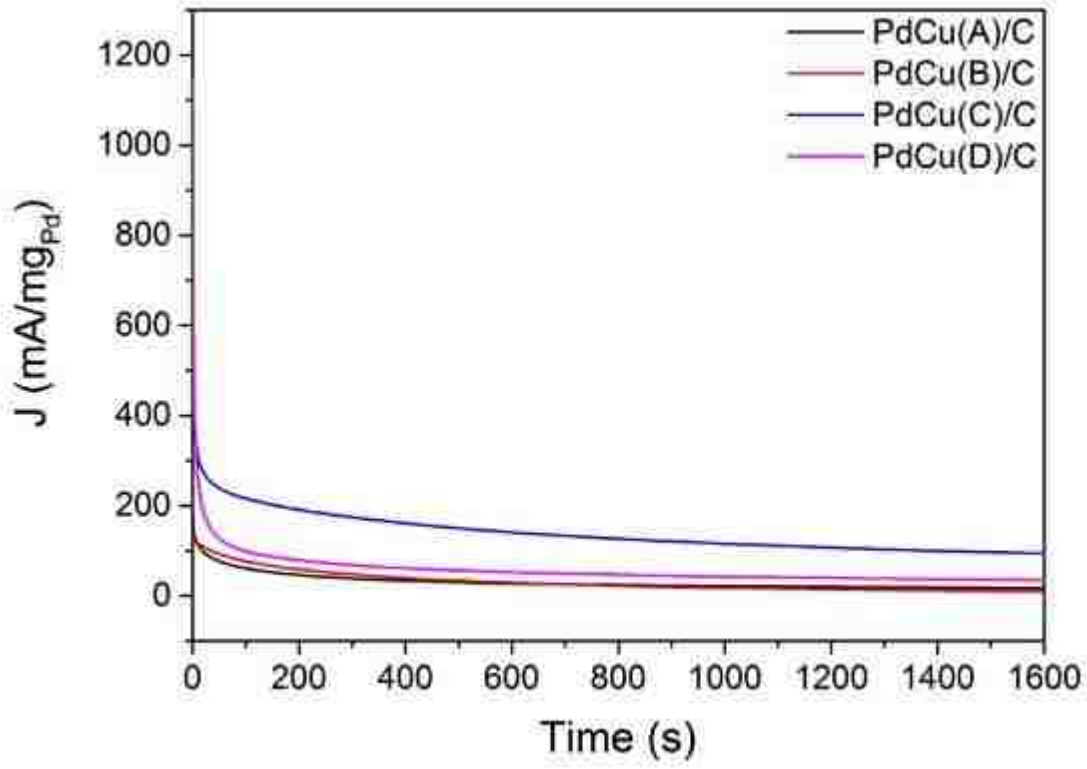

Figure 3-9. i-t curves for Pd-Cu samples in 0.1 NaOH + 1 M ethanol at 0.8 V vs RHE: Pd-Cu(A)/C (black); Pd-Cu(B)/C (red); Pd-Cu(C)/C (green); Pd-Cu(D)/C (blue).

The stability of catalysts was assessed by CV sweeps from 0 – 1.4 V vs RHE at a scan rate of 50 mV/s in 0.1 M NaOH + 1 M ethanol. The CV curves were measured before and after 500 cycles scan. The differences of current densities and positions of oxidation peaks can be

compared (Figure 3-10). In previous reports,[32,33] Pd dissolution was observed in the accelerated stability test; therefore, it is expected that the current densities decease due to the loss of active Pd during the catalytic processes.[34] Based on our results, Pd-Cu(D)/C showed the decrease of current density which is in agreement with reported results,[16,34] while others showed an increase of current densities. In addition, oxidation peak for all samples shifted to more positive potentials. The increase of current density could be explained as the removal of the surface ligands and partial dissolution of Pd containing inactive atoms. In other words, duration test with hundreds of CV sweeps generated more active sites available for EOR, thereby increasing the current density of the oxidation. It is worth noting that initial Pd(B)/C and Pd-Cu(C)/C showed to some degree CO resistance, but after 500 cycling the J_b became lager than J_f, suggesting the decreased ability of the resistance to CO.

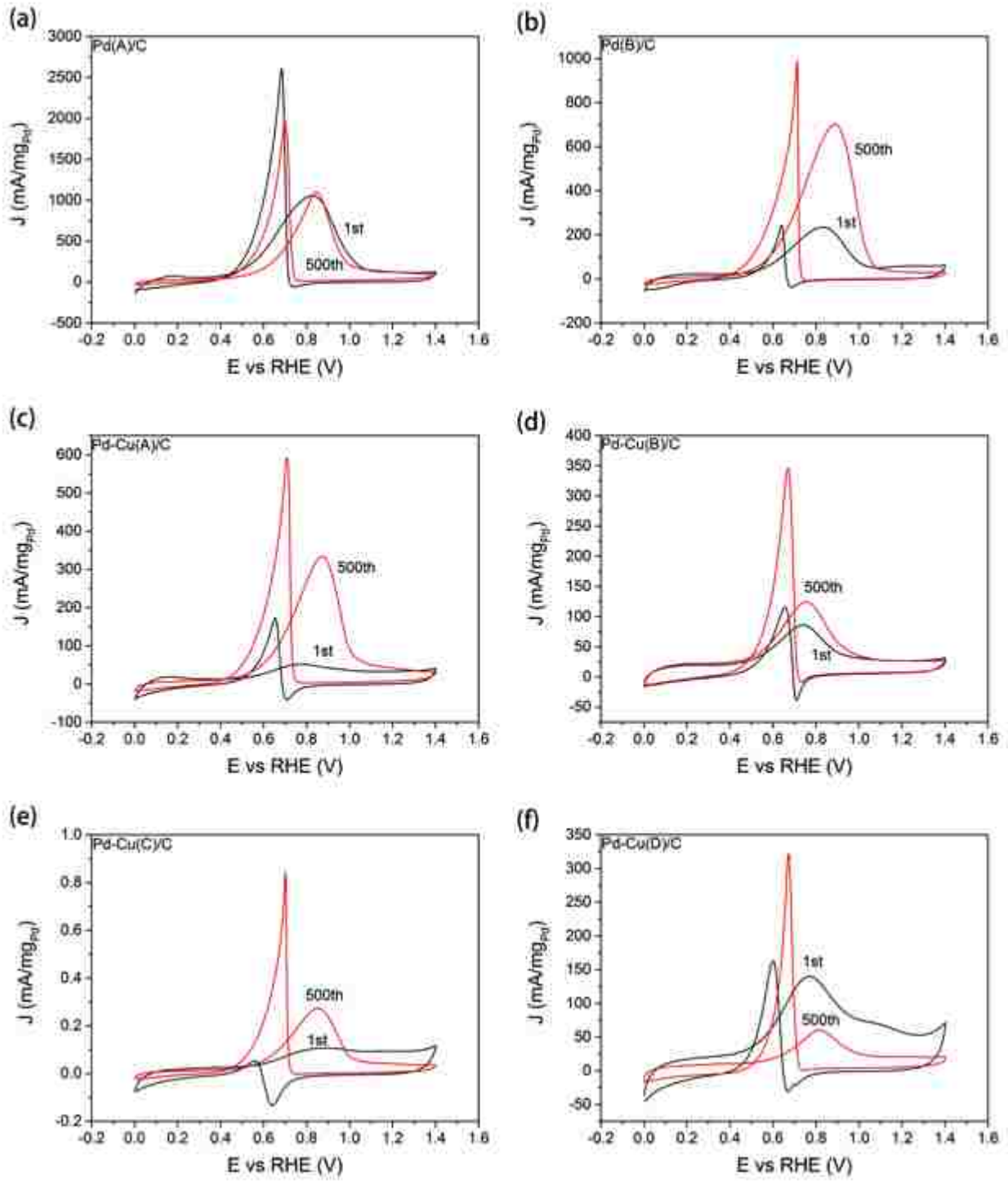

Figure 3-10. Stability tests of Pd and Pd-Cu catalysts for EOR in 0.1 NaOH + 1 M ethanol from 0 to 1.4 V RHE at a scan rate of 50 mV/s: (a) Pd(A)/C, (b) Pd(B)/C, (c) Pd-Cu(A)/C; (d) Pd-Cu(B)/C; (e) Pd-Cu(C)/C; and (f) Pd-Cu(D)/C.

3.4 Conclusion

Pd and Pd-Cu nanostructures synthesized by different reducing agents have been tested on the electrocatalytic performances for EOR. The ECSA was determined by integrating the PdO peak. The results show Pd and Pd-Cu nanostructures have very large ECSAs. In EOR tests, Pd and Pd-Cu nanostructures show high peak specific current densities (~ 400 mA/mg_{Pd}), which are close to some Pt based catalysts.[35] Meanwhile, it was found that values of J_f/J_b of samples could grow with increase of scan rates. In i-t tests, smaller sizes samples show stronger tolerance to CO, since their much larger surface areas and catalytically more active sites. For duration test, except Pd-Cu(D)/C, all the other samples showed unusual increase of current density, which indicates their high stability as EOR catalysts. Further understanding of reaction mechanism is needed in future experiments.

3.5 Reference

(1) Yin, J.; Shan, S.; Ng, M. S.; Yang, L.; Mott, D.; Fang, W.; Kang, N.; Luo, J.; Zhong, C.-J. *Langmuir* **2013**, *29*, 9249.

(2) Xu, C.; Liu, Y.; Wang, J.; Geng, H.; Qiu, H. *Journal of Power Sources* **2012**, *199*, 124.

(3) Xu, C.; Zhang, Y.; Wang, L.; Xu, L.; Bian, X.; Ma, H.; Ding, Y. *Chemistry of Materials* **2009**, *21*, 3110.

(4) Guo, S.; Zhang, S.; Sun, X.; Sun, S. *Journal of the American Chemical Society* **2011**, *133*, 15354.

(5) Witońska, I. A.; Walock, M. J.; Dziugan, P.; Karski, S.; Stanishevsky, A. V. *Applied Surface Science* **2013**, *273*, 330.

(6) Chen, S.; Jenkins, S. V.; Tao, J.; Zhu, Y.; Chen, J. *The Journal of Physical Chemistry C* **2013**, *117*, 8924.

(7) Kolmakov, A.; Klenov, D. O.; Lilach, Y.; Stemmer, S.; Moskovits, M. *Nano Letters* **2005**, *5*, 667.

(8) Bianchini, C.; Shen, P. K. *Chemical Reviews* **2009**, *109*, 4183.

(9) Liang, Z. X.; Zhao, T. S.; Xu, J. B.; Zhu, L. D. *Electrochimica Acta* **2009**, *54*, 2203.

(10) Cui, G.; Song, S.; Shen, P. K.; Kowal, A.; Bianchini, C. *The Journal of Physical Chemistry C* **2009**, *113*, 15639.

(11) Yajima, T.; Wakabayashi, N.; Uchida, H.; Watanabe, M. *Chemical Communications* **2003**, 828.

(12) Ksar, F.; Ramos, L.; Keita, B.; Nadjo, L.; Beaunier, P.; Remita, H. *Chemistry of Materials* **2009**, *21*, 3677.

(13) Qiu, X.; Dai, Y.; Tang, Y.; Lu, T.; Wei, S.; Chen, Y. *Journal of Power Sources* **2015**, *278*, 430.

(14) Huang, Y.; Guo, Y.; Wang, Y.; Yao, J. *International Journal of Hydrogen Energy* **2014**, *39*, 4274.

(15) Neto, A. O.; Tusi, M. M.; de Oliveira Polanco, N. S.; da Silva, S. G.; Coelho dos Santos, M.; Spinacé, E. V. *International Journal of Hydrogen Energy* **2011**, *36*, 10522.

(16) Hu, C.; Cheng, H.; Zhao, Y.; Hu, Y.; Liu, Y.; Dai, L.; Qu, L. *Advanced Materials* **2012**, *24*, 5493.

(17) Jiang, R.; Tran, D. T.; McClure, J. P.; Chu, D. *ACS Catalysis* **2014**, *4*, 2577.

(18) Kakaei, K.; Dorraji, M. *Electrochimica Acta* **2014**, *143*, 207.

(19) Hu, C.; Zhai, X.; Zhao, Y.; Bian, K.; Zhang, J.; Qu, L.; Zhang, H.; Luo, H. *Nanoscale* **2014**, *6*, 2768.

(20) Mukherjee, P.; Roy, P. S.; Mandal, K.; Bhattacharjee, D.; Dasgupta, S.; Bhattacharya, S. K. *Electrochimica Acta* **2015**, *154*, 447.

(21) Trasatti, S.; Petrii, O. A. In *Pure and Applied Chemistry* 1991; Vol. 63, p 711.

(22) Higuchi, K.; Yamamoto, K.; Kajioka, H.; Toiyama, K.; Honda, M.; Orimo, S.; Fujii, H. *Journal of Alloys and Compounds* **2002**, *330–332*, 526.

(23) Sakintuna, B.; Lamari-Darkrim, F.; Hirscher, M. *International Journal of Hydrogen Energy* **2007**, *32*, 1121.

(24) Correia, A. N.; Mascaro, L. H.; Machado, S. A. S.; Avaca, L. A. *Electrochimica Acta* **1997**, *42*, 493.

(25) Xu, R.; Groot, R. A. d.; Lugt, W. v. d. *Journal of Physics: Condensed Matter* **1992**, *4*, 2389.

(26) Lan-lan, F.; Qian, T.; Ming-fang, L.; Ling-wen, L.; Dong, C.; Yan-xia, C. *Chinese Journal of Chemical Physics* **2010**, *23*, 543.

(27) Xiao, L.; Zhuang, L.; Liu, Y.; Lu, J.; Abruña, H. D. *Journal of the American Chemical Society* **2009**, *131*, 602.

(28) Wang, Y.; He, Q.; Ding, K.; Wei, H.; Guo, J.; Wang, Q.; O'Connor, R.; Huang, X.; Luo, Z.; Shen, T. D.; Wei, S.; Guo, Z. *Journal of The Electrochemical Society* **2015**, *162*, F755.

(29) Zhang, Z.; Xin, L.; Sun, K.; Li, W. *International Journal of Hydrogen Energy* **2011**, *36*, 12686.

(30) Fernández-García, M.; Conesa, J. C.; Clotet, A.; Ricart, J. M.; López, N.; Illas, F. *The Journal of Physical Chemistry B* **1998**, *102*, 141.

(31) Lou, Y.; Maye, M. M.; Han, L.; Luo, J.; Zhong, C.-J. *Chemical Communications* **2001**, 473.

(32) qukaszewski M; A., C. s. *J Solid State Electrochem* **2008**, *12*, 1589.

(33) Rand DAJ; R., W. *Electroanal Chem* **1972**, *35*, 209.

(34) Xu, J. B.; Zhao, T. S.; Shen, S. Y.; Li, Y. S. *International Journal of Hydrogen Energy* **2010**, *35*, 6490.

(35) Liu, B.; Chen, J. H.; Zhong, X. X.; Cui, K. Z.; Zhou, H. H.; Kuang, Y. F. *Journal of Colloid and Interface Science* **2007**, *307*, 139.

4. Conclusion

Different sizes and shapes of Pd and Pd-Cu nanostructures were successfully synthesized by using the two reducing agents (i.e., L-ascorbyl-6-palmitate and phenylphosphinic acid) through chemical reduction reaction. The process of formation of Pd and Pd-Cu is thought to be two steps reaction. In the first step, the Pd precursor form Pd seed; in second step, the seeds grow to final Pd or Pd-Cu structures. Pd nanostructures synthesized by L-ascorbyl-6-palmitate trended to exhibit irregular branch shapes or rod like shapes in large sizes. In contrast, phenylphosphinic acid favored to form spherical and uniform sizes Pd nanostructures. Pd particles synthesized by phenylphosphinic acid had smaller average size of 4.15 nm compared to those reduced by L-ascorbyl-6-palmitate with average size of 10.52 nm. The Pd-Cu samples displayed similar tendency as pure Pd nanostructures by using these two reducing agents in the syntheses. By comparing results from different Cu precursors (e.g. $Cu(acac)_2$ and $CuCl_2$), it was found that particles reduced from $CuCl_2$ have larger sizes than those reduced from $Cu(acac)_2$ because Cl^- increases redox potential of Cu resulting in slow reduction of Cu. Furthermore, the reducing agents play important roles to control composition of alloys. The ICP-MS results showed that at a fixed Pd/Cu ratio phenylphosphinic acid favored to increase the percentage of Cu in Pd-Cu system. Further characterization by XPS and HR-TEM can be employed in order to understand the growth mechanism.

These Pd and Pd-Cu nanostructures have further been tested for application as catalysts for EOR in fuel cells. The ECSAs of Pd and Pd-Cu nanostructures were estimated by oxygen adsorption and desertions on Pd. Compared to pervious catalysts, those catalysts displayed extremely large ECSAs, especially the sample Pd-Cu(C)/C with 18229.82 $m^2/g_{Pd.}$ The results of EOR tests showed that these catalysts had high specific current densities. Meanwhile, Pd-Cu

catalysts showed to some certain extent resistance against CO-like intermediates by examining J_f/J_b. The resistance showed a relationship with the sizes of Pd particles. The smaller particles exhibited better ability against CO-like intermediates. Most samples showed high stabilities even after 500 cycles scan.